

Relativistic effects in Lyman- α forest

Vid Iršič,^a Enea Di Dio,^{b,c} Matteo Viel^{b,c}

^aThe Abdus Salam International Centre for Theoretical Physics, Strada Costiera 11, I-34151 Trieste, Italy

^bINAF - Osservatorio Astronomico di Trieste, Via G. B. Tiepolo 11, I-34143 Trieste, Italy

^cINFN-National Institute for Nuclear Physics, via Valerio 2, I-34127 Trieste, Italy

E-mail: virsic@ictp.it, enea.didio@oats.inaf.it, viel@oats.inaf.it

Abstract. We present the calculation of the Lyman-alpha (Lyman- α) transmitted flux fluctuations with full relativistic corrections to the first order. Even though several studies exist on relativistic effects in galaxy clustering, this is the first study to extend the formalism to a different tracer of underlying matter at unique redshift range ($z = 2 - 5$). Furthermore, we show a comprehensive application of our calculations to the Quasar-Lyman- α cross-correlation function. Our results indicate that the signal of relativistic effects are sizeable at Baryonic Acoustic Oscillation (BAO) scale mainly due to the large differences in density bias factors of our tracers. We construct an observable, the anti-symmetric part of the cross-correlation function, that is dominated by the relativistic signal and offers a new way to measure the relativistic terms at relatively small scales. The analysis shows that relativistic effects are important when considering cross-correlations between tracers with very different biases, and should be included in the data analysis of the current and future surveys. Moreover, the idea presented in this paper is highly complementary to other techniques and observables trying to isolate the effect of the relativistic corrections and thus test the validity of the theory of gravity beyond the Newtonian regime.

Contents

1	Introduction	1
2	Ly-α absorption	2
3	Ly-α observable	3
3.1	Quasar density fluctuations	6
3.2	Non-linear corrections	6
3.3	Biases	8
4	2-point correlation function	10
4.1	Local term expansion in \mathcal{H}/k	15
4.2	Symmetric correlation function	17
4.3	Anti-symmetric correlation function	18
4.4	Signal-to-noise analysis	24
4.5	Discussion on systematic effects	27
5	Conclusions	29
A	Angular power spectrum	30
B	CLASS modifications	32

1 Introduction

The last decade has witnessed an enormous progress in the cosmological investigation of the intergalactic medium (IGM) as probed by the Lyman- α forest (see [1, 2] for reviews). In particular, the Lyman- α forest is now a viable cosmological observable that can help in putting constraints on cosmological parameters and/or deviations from a standard scenario based on Cold Dark Matter (CDM) and a cosmological constant. More recently, the very large number of quasar spectra of the SDSS-III/BOSS (Sloan Digital Sky Survey-III/Baryon Oscillation Spectroscopic Survey) collaboration using a state-of-the-art analysis, has allowed to discover Baryonic Acoustic Oscillations (BAOs) in the transmitted Lyman- α flux at $z \sim 2.3$ [3, 4]: this spectacular confirmation of the cosmological nature of the Lyman- α forest was mainly made possible by exploiting the flux correlations in three dimensions out to large scales. Moreover, the one-dimensional analysis of the transmitted flux power has allowed to place the most stringent bounds on total neutrino mass and cold dark matter coldness by using spectra at high and low resolution [5–7].

The first steps have also been taken in measuring the cross-correlations between various different observables in the same volume of the survey. Such examples include the cross-correlations between the Lyman- α forest and Damped Lyman- α systems [8]

and the Lyman- α forest and Quasars (QSOs) [9, 10]. The first measurements measured the correlations up to the BAO scale and confirmed the location of the peak, however the error bars remain large. Nevertheless, the analysis was done on barely half of the available data by the SDSS-III/BOSS survey and future generation of large-scale structure surveys (e.g. SDSS-IV/eBOSS [11], DESI [12], etc.) are going to improve on the precision of the measurements to a percent level thus forcing the theoretical models to match unprecedented demanding constraints in terms of accuracy.

However, as the observations move out to larger scales the validity of a simple Newtonian description starts to come into question. Recent years have seen a lot of effort put into understanding and possibly measuring the signal of relativistic effects and/or weak gravitational lensing in the 2-point statistics of the galaxy clustering, see e.g. [13–21]. Moreover, it has been speculated that the most powerful tool for such an analysis would be the cross-correlations between different galaxy populations [13, 14, 16, 18, 20, 21]. The correlation of two differently biased tracers of the underlying matter field will, at least to the first order, boost the signal of the beyond-Kaiser effects relative to the difference in the density bias factors. Thus the larger the difference the stronger the signal. Unfortunately the difference in density bias factors among different galaxy populations is relatively small, and the idea has only received attention very recently.

On the other hand, the tracers such as Lyman- α forest or QSOs that are measured in the same survey volume by already existing surveys are very differently biased tracers. Exploiting this difference would boost the signal of the relativistic effects to a measurable level. Given the highly non-linear relation between the observed Lyman- α forest flux fluctuations and the underlying density field, one might question the ability to use the Lyman- α forest as a linear tracer. However, several studies have shown that on large scales Lyman- α forest behaves as any other local tracer and any deviations start to show up at smaller scales [22–24].

In this paper we compute the theoretical predictions for the QSO-Lyman- α cross-correlation function and show how the difference in the density biases of the two tracers boosts the signal of the relativistic effects to a 10% level above scales of $\sim 40 h^{-1}\text{Mpc}$. The paper is structured as follows: in Sections 2 and 3 we introduce the Lyman- α forest observable and derive the flux fluctuations using fully relativistic treatment. In Section 4 we apply the calculations to the QSO-Lyman- α cross-correlation function and present the results for both symmetric and anti-symmetric parts. We conclude in Section 5.

2 Ly- α absorption

The Lyman- α forest is an absorption feature seen in the spectra of high redshift QSO and galaxies and is a unique tracer of the underlying matter distribution in the redshift range of $z = 2 - 5$.

When the light from a distant QSO passes through the intergalactic medium (IGM), the neutral hydrogen along the line of sight will cause absorption of the QSO continuum by the redshifted Lyman- α (121.565 nm) resonance line. The collection of this absorption lines blend into one feature called the Lyman- α forest. In fact it is more correct to think

of the Lyman- α forest as being caused by continuous absorption of the mildly fluctuating density of the IGM.

Observed transmission of the flux is thus a tracer of the baryon distribution of the IGM and one of the successes of the Lyman- α in the last few years has been to establish it as a precision cosmology probe.

The photons' absorption due to Lyman- α is described by the differential equation

$$d \ln \mathcal{N}_\gamma = -A n_{\text{HI}} \phi(E, E_\alpha) dt \quad (2.1)$$

where E_α is the Lyman- α absorption line, \mathcal{N}_γ the photon occupation number, t the proper time in absorption HI rest frame and n_{HI} the number density of neutral hydrogen. A is a physical constant derived from Einstein coefficients and given by $A = e^2 f_\alpha / 4 \epsilon_0 m_e$, where e is the electron charge, ϵ_0 is vacuum permittivity, m_e electron mass and $f_\alpha = 0.4164$ oscillation strength of the Lyman- α transition. The integral of the absorption line profile ($\phi(E, E_\alpha)$) over the energy is normalized to the unity. We define the optical depth as

$$\tau \equiv \int_{\text{light-cone}} d \ln \mathcal{N}_\gamma. \quad (2.2)$$

The above definition agrees with the non-relativistic result in the appropriate limit.

3 Ly- α observable

On large scales we can work under the approximation that $\phi(E, E_\alpha) = \delta_D(E - E_\alpha)$. Hence, we neglect thermal broadening which affects scales of $10 h^{-1}$ Mpc. This approximation is valid as long as we are interested in large scale correlations. Therefore, our observable is the transmitted flux fraction F , i.e. the photon occupation number observed normalized with the emitted one, which yields to

$$F = e^{-\tau}, \quad (3.1)$$

in terms of the measured angle¹ \mathbf{n} and redshift z , corresponding to the shift in the Lyman- α spectrum (i.e. $1 + z = E_\alpha/E$), namely $F(\mathbf{n}, z)$. One can define the fluctuations of the transmitted flux as

$$\delta_F(\mathbf{n}, z) \equiv \frac{F(\mathbf{n}, z)}{\langle F(\mathbf{n}, z) \rangle} - 1, \quad (3.2)$$

where $\langle \cdot \rangle$ denotes the angular mean at fixed observed redshift z .

On large scales, we can linearize the relation between the transmitted flux and the optical depth and express the observable quantity as

$$\delta_F(\mathbf{n}, z) = -(\tau(\mathbf{n}, z) - \langle \tau(\mathbf{n}, z) \rangle) \equiv -\delta\tau(\mathbf{n}, z). \quad (3.3)$$

¹We follow the notation of Ref. [25], where \mathbf{n} denotes the direction of propagation of the photon. Hence the measured angle is $-\mathbf{n}$, but for sake of simplicity will refer to \mathbf{n} as argument of the observable quantities.

The linearization of the exponential in Eq. (3.1) might question the validity of the perturbative approach. Nevertheless, as shown in section 3.2, one can expand perturbatively the transmitted flux F in terms of the optical depth τ by introducing some bias factors which encode the effect of the mode coupling.

From Eqs. (2.1) and (2.2) we obtain

$$\begin{aligned}\tau(\mathbf{n}, z) &= -A \int n_{\text{HI}} \delta_D(E - E_\alpha) dt = -A \int n_{\text{HI}} \delta_D(E^{\text{obs}}(1+z) - E_\alpha) dt \\ &= -A \int \frac{n_{\text{HI}}}{E^{\text{obs}}} \delta_D\left((1+z) - \frac{E_\alpha}{E^{\text{obs}}}\right) \frac{dt}{dz} dz = -A n_{\text{HI}} \frac{1+z}{E_\alpha} \frac{dt}{dz}\end{aligned}\quad (3.4)$$

where all quantities are evaluated at $1+z = E_\alpha/E_{\text{obs}}$ and the suffix 'obs' denotes quantities evaluated with respect to the observer rest frame and t is the proper time² in the photons absorption frame.

In this section we aim to derive Eq. (3.3) to first order in perturbation theory. As long as we describe observable quantities, we have the freedom to work in any gauge without loss of generality. We choose to work in Newtonian gauge $d\bar{s}^2 = a^2 ds^2$, where a is the scale factor of the universe and

$$d\bar{s}^2 = -(1+2\Psi) d\eta^2 + (1-2\Phi) \delta_{ij} dx^i dx^j \quad (3.5)$$

is the conformal metric, where the metric perturbations Ψ and Φ are the Bardeen potentials. From Eq. (3.4), we need to compute $\frac{dt}{dz}$ to first order in perturbation theory

$$\begin{aligned}\frac{dt}{dz} &= \frac{dt}{d\eta} \frac{d\eta}{dz} = \frac{dt}{d\eta} \frac{d\eta}{dz} = \frac{1+\Psi}{1+\bar{z}} \left(\frac{d\bar{z}}{d\eta} + \frac{d\delta z}{d\eta} \right)^{-1} \\ &= \frac{1+\Psi}{1+\bar{z}} \left(\frac{d\bar{z}}{d\eta} \left(1 + \frac{\delta z}{1+z} \right) + (1+z) \frac{d}{d\eta} \left(\frac{\delta z}{1+z} \right) \right)^{-1} \\ &= -\frac{1+\Psi}{\mathcal{H}(\bar{z})(1+\bar{z})^2} \left[1 - \frac{\delta z}{1+z} + \frac{1}{\mathcal{H}} \frac{d}{d\eta} \left(\frac{\delta z}{1+z} \right) \right] \\ &= -\frac{1}{\mathcal{H}(1+z)^2} \left[1 + \Psi + \left(1 - \frac{\dot{\mathcal{H}}}{\mathcal{H}^2} \right) \frac{\delta z}{1+z} + \frac{1}{\mathcal{H}} \frac{d}{d\eta} \left(\frac{\delta z}{1+z} \right) \right] \\ &= -\frac{1}{\mathcal{H}(1+z)^2} \left[1 + \Psi + \left(1 - \frac{\dot{\mathcal{H}}}{\mathcal{H}^2} \right) \frac{\delta z}{1+z} + \mathbf{n} \cdot \mathbf{v} + \mathcal{H}^{-1} \partial_r \mathbf{n} \cdot \mathbf{v} + \mathcal{H}^{-1} \dot{\Phi} \right],\end{aligned}\quad (3.6)$$

where $\mathcal{H} = \dot{a}/a$ is the comoving Hubble parameter and a dot denotes the derivative with respect to the conformal time η . We have also introduced the unperturbed redshift \bar{z} by expanding the observed redshift as $z = \bar{z} + \delta z$. In general, in this work, we will denote with an overbar background quantities in perturbation theory. In the last equality we have assumed that sources move along geodesic

$$\mathbf{n} \cdot \dot{\mathbf{v}} + \mathcal{H} \mathbf{n} \cdot \mathbf{v} - \partial_r \Psi = 0, \quad (3.7)$$

²We prefer not to denote the proper time with τ to avoid confusion with the optical depth.

and used

$$\frac{\delta z}{1+z} = - \left(\Psi + \mathbf{n} \cdot \mathbf{v} + \int_{\eta}^{\eta_0} (\dot{\Psi} + \dot{\Phi}) d\eta' \right), \quad (3.8)$$

which is derived from geodesic equation. We remind that the physical density of HI, i.e. $n_{\text{HI}}(z)$ in Eq. (3.4), is related to the density computed in perturbation theory to first order as

$$n_{\text{HI}}(z) = \bar{n}_{\text{HI}}(z) \left(1 - \frac{d \ln \bar{n}_{\text{HI}}}{dz} \delta z + \delta_{\text{HI}} \right). \quad (3.9)$$

The second term in the brackets describes the source evolution and it is often parametrized through the evolution bias

$$f_{\text{evo}}^{\text{Ly}\alpha} \equiv \frac{\partial \ln (a^3 \bar{n}_{\text{HI}})}{\mathcal{H} \partial \eta} = 3 - (1+z) \frac{d \ln \bar{n}_{\text{HI}}}{dz}. \quad (3.10)$$

Finally, we find

$$\begin{aligned} \tau(\mathbf{n}, z) = \bar{\tau}(z) \left[1 + \delta_{\text{HI}}^{\text{sync}} + \mathcal{H}^{-1} \partial_r \mathbf{n} \cdot \mathbf{v} - \left(2 + \frac{\dot{\mathcal{H}}}{\mathcal{H}^2} - f_{\text{evo}}^{\text{Ly}\alpha} \right) \frac{\delta z}{1+z} \right. \\ \left. + \mathbf{n} \cdot \mathbf{v} + \Psi + \mathcal{H}^{-1} \dot{\Phi} + (f_{\text{evo}}^{\text{Ly}\alpha} - 3) \mathcal{H} v \right]. \end{aligned} \quad (3.11)$$

where

$$\bar{\tau}(z) \equiv \frac{A}{E_{\alpha}} \frac{\bar{n}_{\text{HI}}}{\mathcal{H} (1+z)} \quad (3.12)$$

and v is the (gauge invariant) velocity potential in Newtonian gauge defined through $\mathbf{v} = -\nabla v$. We have also expressed the density perturbation in synchronous gauge, through $\delta^{\text{sync}} = \delta + (3 - f_{\text{evo}}) \mathcal{H} v$.

The unperturbed optical depth $\bar{\tau}$ can be rewritten as ([24]):

$$\bar{\tau}(z) = \frac{A \bar{n}_{\text{HI}}}{E_{\alpha} H} \approx 1.27 \times \frac{10^{-12} \text{s}^{-1}}{\Gamma_{\gamma, \text{HI}}} \left(\frac{X}{0.75} \right)^2 \left(\frac{T_0}{10^4 \text{K}} \right)^{-0.7} \frac{\omega_{b,0}^2}{h} \frac{H_0}{H} (1+z)^6, \quad (3.13)$$

where T_0 is the mean temperature of the gas and we have used the mass fraction of neutral hydrogen through the photo-ionization equilibrium

$$n_{\text{HI}} = n_H^2 \frac{\alpha(T)}{\Gamma_{\gamma, \text{HI}}} = \frac{X^2 \rho_b^2 \alpha(T)}{m_H^2 \Gamma_{\gamma, \text{HI}}}. \quad (3.14)$$

where $\Gamma_{\gamma, \text{HI}}$ is the photo-ionization rate, X is the hydrogen mass fraction, n_H is the hydrogen number density, m_H is the hydrogen mass, ρ_b is the baryon energy density and the recombination rate $\alpha(T)$ is given by

$$\alpha(T) = \alpha_0 \left(\frac{T}{10^4 \text{K}} \right)^{-0.7}, \quad (3.15)$$

where $\alpha_0 = 4.3 \times 10^{-13} \text{s}^{-1} \text{cm}^3$.

In this work we consider the Planck best fit cosmological parameters [26], namely $\omega_{b,0} = 0.022$, $h = 0.67$ and the astrophysical parameters $T_0 = 1.47088 \times 10^4$ K, $X = 0.75$ and $\Gamma_{\gamma,\text{HI}} = 10^{-12} s^{-1}$. With these parameters Eq. (3.13) reduces to

$$\bar{\tau}(z) \approx 7 \times 10^{-4} \frac{(1+z)^6}{E(z)} \quad (3.16)$$

with $E(z) = H(z)/H_0$.

3.1 Quasar density fluctuations

In the following of this paper we will be interested in cross-correlating the Lyman- α signal with the quasar density fluctuations. In the light of that we give an expression with relativistic corrections used for the QSO fluctuations as found in the literature, and used in this paper.

The number counts for discrete tracers has been derived in [25, 27] in galaxy clustering framework. Nevertheless their results can be applied as well to QSOs, just considering the appropriate bias factors,

$$\begin{aligned} \Delta_Q(\mathbf{n}, z) = & b_Q \delta^{\text{sync}} + (5s - 2)\Phi + \Psi + \frac{1}{\mathcal{H}} \left[\dot{\Phi} + \partial_r(\mathbf{n} \cdot \mathbf{v}) \right] + (f_{\text{evo}}^Q - 3) \mathcal{H}v \\ & + \left(\frac{\dot{\mathcal{H}}}{\mathcal{H}^2} + \frac{2 - 5s}{r_S \mathcal{H}} + 5s - f_{\text{evo}}^Q \right) \left(\Psi + \mathbf{n} \cdot \mathbf{v} + \int_0^{r_S} dr (\dot{\Phi} + \dot{\Psi}) \right) \\ & + \frac{2 - 5s}{2r_S} \int_0^{r_S} dr \left[2 - \frac{r_S - r}{r} \Delta_\Omega \right] (\Phi + \Psi). \end{aligned} \quad (3.17)$$

Differently from Lyman- α forest, single tracer number counts include a cosmic magnification contribution and a magnification bias parameter s defined as

$$s = - \frac{2}{5} \frac{\partial \ln \bar{n}(z, \ln L)}{\partial \ln L} \Big|_{\bar{L}} \quad (3.18)$$

where \bar{L} denotes the threshold luminosity of the survey and \bar{n} is the background number density. Similarly, the evolution bias factor of QSOs is related to the QSO number density distribution (see Eq. (3.10)).

3.2 Non-linear corrections

In the previous section we have computed the optical depth $\tau(z)$ to first order in perturbation theory. However, the exponential (3.1) introduces a mode coupling that we neglect by linearizing this expression. In the context of the relativistic corrections beyond simple Kaiser approximation this is valid if the terms themselves are small.

In this section we give an estimation of the bias for the relativistic terms (mainly Doppler term as it is largest). We use the formalism described in [28, 29], and extend it to capture relativistic correction described in this paper. We do not use this linear description to try to describe the density bias.

If the terms are not small, a correction capturing the non-linearity of the $F - \tau$ transformation is applied in terms of bias factors, as is the case with the redshift-space distortions. The full calculation for the velocity-gradient bias factor can be found in the literature ([28, 29]), but we will review the basic steps here for clarity. To the leading order, the relativistic corrections enter our Lyman- α calculations only through the change of coordinates, from the real space time (radial coordinate) to a redshift (redshift-space coordinate) as can be seen from Eqs. 3.4-3.6. Neglecting for the moment the relativistic corrections and focusing only on the velocity-gradient part, we see that the observed optical depth can be written as

$$\tau(\mathbf{n}, z) = \bar{\tau} (1 + \delta)^p (1 + \mathcal{H}^{-1} \partial_r \mathbf{n} \cdot \mathbf{v}), \quad (3.19)$$

where the value of p is usually taken in the range $\sim 1.5 - 1.7$ [28], and δ is the non-linear density fluctuations. From here one can define an optical depth bias with respect to the redshift-space distortions as

$$b_{\tau,v} \equiv \frac{1}{\langle \tau \rangle} \left\langle \frac{\partial \tau}{\partial (\mathcal{H}^{-1} \partial_r \mathbf{n} \cdot \mathbf{v})} \right\rangle = 1. \quad (3.20)$$

This is not a new result, indeed it tells us that there is no velocity-gradient bias, as one would expect. However, the observable of the Lyman- α forest is not the optical depth but the flux, and the non-linear transformation is applied after the redshift-space distortions. One can write the flux bias of the velocity-gradient as

$$\begin{aligned} b_{F,v} &\equiv \frac{1}{\langle F \rangle} \left\langle \frac{\partial F}{\partial (\mathcal{H}^{-1} \partial_r \mathbf{n} \cdot \mathbf{v})} \right\rangle = \frac{1}{\langle F \rangle} \left\langle \frac{\partial F}{\partial (\mathcal{H}^{-1} \partial_r \mathbf{n} \cdot \mathbf{v})} \right\rangle = \\ &= \frac{1}{\langle F \rangle} \left\langle \frac{\partial F}{\partial \tau} \frac{\partial \tau}{\partial (\mathcal{H}^{-1} \partial_r \mathbf{n} \cdot \mathbf{v})} \right\rangle = \frac{1}{\langle F \rangle} \left\langle \frac{\partial F}{\partial \tau} \tau \right\rangle = \\ &= \frac{\langle F \ln F \rangle}{\langle F \rangle}. \end{aligned} \quad (3.21)$$

This result has been first obtained by [28] and has been further shown to work extremely well in the absence of thermal smoothing ([29]).

The above review calculation was done using redshift-space distortions only, as written in Eq. 3.19. However there is no reason the same calculation can be carried out in the same manner if one replaces $\mathcal{H}^{-1} \partial_r \mathbf{n} \cdot \mathbf{v}$ with any other quantity, e.g. a relativistic doppler term ($\mathbf{n} \cdot \mathbf{v}$). In such a case one would modify the optical depth relation as

$$\tau(\mathbf{n}, z) = \bar{\tau} (1 + \delta)^p \left(1 + \mathcal{H}^{-1} \partial_r \mathbf{n} \cdot \mathbf{v} + \left(3 - f_{\text{evo}}^{\text{Ly}\alpha} + \frac{\dot{\mathcal{H}}}{\mathcal{H}^2} \right) \mathbf{n} \cdot \mathbf{v} \right). \quad (3.22)$$

Accordingly the optical depth bias, with respect to Doppler term would now be

$$b_{\tau,D} \equiv \frac{1}{\langle \tau \rangle} \left\langle \frac{\partial \tau}{\partial (\mathbf{n} \cdot \mathbf{v})} \right\rangle = 3 - f_{\text{evo}}^{\text{Ly}\alpha} + \frac{\dot{\mathcal{H}}}{\mathcal{H}^2}, \quad (3.23)$$

and since the $b_{\tau,D}$ is a constant it furthermore means

$$b_{F,D} = b_{\tau,D} \frac{\langle F \ln F \rangle}{\langle F \rangle} = b_{\tau,D} b_{F,v}. \quad (3.24)$$

Thus any kind of scaling of the redshift coordinate that is linearly added to the redshift space distortions acquires the same (flux) bias factor due to non-linear transformation between the flux and the optical depth, with a pre-factor that is nothing else but the optical depth bias factor for the same quantity.

The above calculation was carried out in the limit of no thermal broadening, since our paper focuses only on the large scale limit. However there is no reason that thermal broadening would distinguish between velocity-gradient effect or Doppler term effect, thus resulting in the same correction to the overall bias factor.

Moreover, in the above model no second order effects were included. In that sense it should be tested on numerical simulations, and only draws on the fact that the leading relativistic effects considered in this paper are nothing less than small corrections to redshift-space transformation, compared to the redshift space distortion. Thus they would behave in the same way under the non-linear transformation. To fully understand the values of the bias factors of the Lyman- α forest a more detailed analysis is required that is beyond the scope of this paper.

Therefore to correctly describe the transmitted flux fluctuation we change the bias factors predicted by the linear theory with the observed bias factors

$$\begin{aligned} \delta_F(\mathbf{n}, z) = & b_\alpha \delta^{\text{sync}} + b_v \mathcal{H}^{-1} \partial_r \mathbf{n} \cdot \mathbf{v} + b_R \left[- \left(2 + \frac{\dot{\mathcal{H}}}{\mathcal{H}^2} - f_{\text{evo}}^{\text{Ly}\alpha} \right) \frac{\delta z}{1+z} \right. \\ & \left. + \mathbf{n} \cdot \mathbf{v} + \Psi + \mathcal{H}^{-1} \dot{\Phi} + (f_{\text{evo}}^{\text{Ly}\alpha} - 3) \mathcal{H} v \right]. \end{aligned} \quad (3.25)$$

The first two terms correspond to a simple Kaiser approximation for the Lyman- α forest tracer, while the terms in the square bracket describe the relativistic corrections. Note that the velocity-gradient bias different than unity is the result of the redshift space distortion acting on the optical depth, before taking the non-linear transformation to the observable which is the flux, and it is not to be interpreted as a violation of the equivalence principle. This result is known and widely used in the literature [22–24, 28]. According to the model presented in this section we adopt a universal bias for all relativistic terms, b_R , which is to the correct description to linear order.

3.3 Biases

In a relativistic framework one has to define the bias parameters with respect the density, and redshift space distortions for Lyman- α forest tracer, in a specific gauge. Indeed, if on small scales the differences between different gauges are generally suppressed by a factor $(\mathcal{H}/k)^2$, on large scales the gauge choice becomes relevant and it might introduce some spurious k -dependences in the bias factors.

However they do not affect the main results of our work which is determined by terms suppressed only by \mathcal{H}/k . Our choice to apply density bias b_α in synchronous

comoving gauge is well justified from the assumption that the tracer and the underlying density perturbation experience the same gravitational field and they move with the same velocity. Hence in their rest frame we can apply the linear bias prescription. In the standard approach the velocity-gradient bias is applied to the Kaiser term, and is derived using Newtonian relation between time derivative of density perturbation and peculiar velocity. If Cold Dark Matter (CDM) is the only species which contributes to energy-momentum tensor perturbations, this relation is equivalent to the linearized Einstein equation provided that the density perturbation is expressed in the synchronous and velocity in the Newtonian gauge. Therefore, to be consistent with standard analysis we used velocity-gradient bias in Newtonian gauge.

In this work we consider the Lyman- α density bias evolution as suggested by the observations ([3, 4, 23, 30])

$$b_\alpha(z) = b_\alpha(z = 2.5) \left(\frac{1+z}{3.5} \right)^{2.9} \quad (3.26)$$

with $b_\alpha(z = 2.5) = -0.15$. For the velocity-gradient bias of the Lyman- α forest we follow the recent work using simulations ([22]) which gives:

$$b_v \equiv \frac{\beta_\alpha(z)b_\alpha(z)}{f(z)}, \quad \beta_\alpha(z) = \beta_\alpha(z = 2.5) \left(\frac{1+z}{3.5} \right)^{-0.86}, \quad (3.27)$$

with the value at the mean redshift $\beta_\alpha(z = 2.5) = 1.36$, and $f = d \ln \delta / d \ln a$ is the growth rate factor.

In addition we have a non-vanishing evolution factor for Lyman- α forest, i.e. $f_{\text{evo}}^{\text{Ly}\alpha} \neq 0$ in Eq. (3.25). Following Eq. (3.10) the value of the Lyman- α evolution bias can be predicted from the redshift evolution of the neutral hydrogen fraction. Using the result of Eq. (3.13), we see that $n_{\text{HI}}(z) \sim \Gamma_{\gamma, \text{HI}}^{-1} T_0^{-0.7} \rho_b^2$. For $\bar{\tau}$, we have followed the calculations of ([24]), and assumed that both UV background radiation ($\Gamma_{\gamma, \text{HI}}$) and the mean temperature of the gas T_0 are constant with redshift, thus resulting in a simple evolution of neutral hydrogen $n_{\text{HI}} \sim (1+z)^6$. In turn this implies a value of $f_{\text{evo}}^{\text{Ly}\alpha} = -3$. This is the value used in the calculations in the remainder of this paper, unless stated otherwise.

Moreover, for the Lyman- α forest, we also have bias of the relativistic terms. Given the definition of such a bias (Eq. 3.24 and 3.25) we use an approximation for its value and say

$$b_R(z) = b_v(z). \quad (3.28)$$

For the QSO density bias factor (b_Q) we use the semi-empirical relation derived by [31, 32]:

$$b_Q(z) = 0.53 + 0.289(1+z)^2 \quad (3.29)$$

The empirical relation fits the observed data very well at lower redshifts and can be safely extrapolated to our mean redshift of $z = 2.5$, giving a value of $b_Q(z = 2.5) \sim 4$, which is a bit high, but in agreement with independent observations at higher redshifts [9, 10, 33].

To derive both the evolution (f_{evo}^Q) and magnification (s) bias parameters we have used a fitting model for Quasar Luminosity Function used in BOSS DR9 data analysis [34]. The assumed threshold absolute magnitude was $\bar{M} = -24.5$. The derived values for the magnification and evolution bias factors are $s = 0.295319$ and $f_{\text{evo}}^Q = 5.7999$.

4 2-point correlation function

Having derived the Lyman- α forest observable and defined the QSO observable we are now interested in studying the 2-point function of the correlation between Lyman- α and QSOs. Namely

$$\xi_{Q\alpha}(z_1, z_2, \theta) \equiv \langle \Delta_Q(\mathbf{n}_1, z_1) \delta_F(\mathbf{n}_2, z_2) \rangle \quad (4.1)$$

where $\cos \theta = \mathbf{n}_1 \cdot \mathbf{n}_2$ and $\Delta_Q(\mathbf{n}, z)$ is the QSO number counts. Equivalently one can define the cross-correlation where the positions of Ly- α and QSO have been exchanged:

$$\xi_{\alpha Q}(z_1, z_2, \theta) \equiv \langle \delta_F(\mathbf{n}_1, z_1) \Delta_Q(\mathbf{n}_2, z_2) \rangle. \quad (4.2)$$

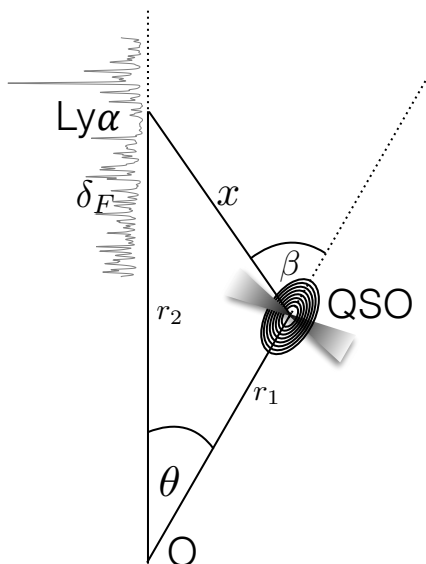


Figure 1. The figure illustrates the correlation between Quasars and Lyman- α forest. The comoving distances of the sources from the observer are denoted by r_1 and r_2 , while x refers to the comoving separation between them.

From Fig. 1 we remark that, by assuming a fiducial cosmology, we can relate the angles β and θ . Hence we can express the correlation functions (4.1, 4.2) in terms of the triplet (z_1, z_2, β) , and we denote them as $\hat{\xi}_{\alpha Q}$ and $\hat{\xi}_{Q\alpha}$. We see directly that the transformation of coordinates ($z_1 \leftrightarrow z_2, \beta \rightarrow \pi - \beta$) maps from one to the other cross-correlation functions, $\hat{\xi}_{Q\alpha}(z_2, z_1, \pi - \beta) = \hat{\xi}_{\alpha Q}(z_1, z_2, \beta)$. While the interchange of the redshifts is obvious, one can see from Fig. 1 that the angle that needs to be flipped is β ,

the angle between the QSO and the pixel in Lyman- α forest, while the angle θ describes their angular separation. The angles are of course connected and either can be used to fully describe the cross-correlation function, however θ is a more natural choice to use with the angular power spectrum expansion (see below).

In general, it is always possible to express the 2-point correlation function in terms of angular power spectra $C_\ell(z_1, z_2)$ as

$$\xi(z_1, z_2, \theta) = \frac{1}{4\pi} \sum_{\ell} (2\ell + 1) C_\ell(z_1, z_2) P_\ell(\cos \theta), \quad (4.3)$$

where P_ℓ denote the Legendre polynomials. In appendix A we introduce the corresponding angular power spectra. Since we are mainly interested in the 1-dimensional correlation function along the radial direction a direct evaluation of Eq. (4.1) is simpler and more intuitive than passing through Eq. (4.3). Nevertheless, we prefer to use Eq. (4.3) to handle the integrated terms (cosmic magnification, integrated Sachs-Wolfe, Shapiro time-delay) and take advantages of CLASS code [35, 36], whose modified transfer functions are shown in appendix B, than rely on approximations.

For the 1-dimensional radial correlation, Eq. (4.1) reduces to a function of two redshifts z_1 and z_2 . It is then convenient to re-express them as a redshift separation between the two source positions $\Delta z = z_1 - z_2$ and a mean redshift $z_{\text{mean}} = (z_1 + z_2)/2$. By assuming a fiducial model we can always map the redshift separation in terms of comoving separation as $x(z_1, z_2) \equiv r(z_1) - r(z_2)$, where

$$r(z) = \int_0^z \frac{dz'}{H(z')} \quad (4.4)$$

is the unperturbed comoving distance and

$$H^2(z) = H_0^2 (a^{-3}\Omega_m + a^{-2}\Omega_K + \Omega_\Lambda). \quad (4.5)$$

We remark that to first order in perturbation theory it is enough to use the background unperturbed redshift-distance relation Eq. (4.4). Because, in general, sources are not homogeneously distributed along the redshift, the 1-dimensional correlation function will not depend only on the absolute value of Δz , or $x(z_1, z_2)$, but on its sign as well.

This change of coordinates simplifies the relation when switching the places of Lyman- α and QSO, $\xi_{\alpha Q}(x, z_{\text{mean}})$ and $\xi_{Q\alpha}(x, z_{\text{mean}})$, since the only transformation required is $x \rightarrow -x$.

Ideally, since the pure radial correlation is described by a single line of sight, the light emitted by a QSO at high redshift would be partially absorbed by the IGM at lower redshift and it will generate the Lyman- α forest absorption lines. This situation is clearly a violation of the photon number conservation assumption on which the derivation (see for instance Ref. [25, 27]) of number counts observable for discrete tracers is based. Nevertheless in our work we never consider this situation and we assume that the two tracers, Lyman- α forest and QSO are correlated gravitationally only. This assumption is consistent with what is done in observations, where the correlation between the Lyman- α forest and the QSO, which produces the absorption lines, is not considered. Another

issue is due to the fact that light emitted by a QSO at high redshift would be affected also by the gravitational potential generated by the Lyman- α forest through the cosmic magnification effect. Being the Lyman- α forest and the QSO on the same line of sight, the impact parameter of the light deflection vanishes and we can not anymore considered it in the weak lensing regime. Since, in any case, exact radial correlation are not taken into consideration we neglect this effect and we describe it as a weak lensing phenomenon. Let us also stress that these possible issues are completely relieved once we consider the dipole with respect to the angle β defined in Fig. 1. Indeed by averaging over all angles the contribution of one single direction has not weight in the integral and its contribution should be negligible. We leave the analysis of the dipole of the correlation function to a future work.

We compute then the full relativistic 2-point correlation function

$$\xi_{Q\alpha} = \xi_{Q\alpha}^{\text{newt}} + \xi_{Q\alpha}^{\text{magnification}} + \xi_{Q\alpha}^{\text{relativistic}} \quad (4.6)$$

where we dropped the dependence on Δz and z_{mean} for simplicity. We start by introducing the primordial curvature power spectrum through

$$\langle R_{\text{in}}(\mathbf{k}) R_{\text{in}}(\mathbf{k}') \rangle = (2\pi)^3 \delta_D^{(3)}(\mathbf{k} + \mathbf{k}') P_R(k) \quad (4.7)$$

and we write any first order variable X in terms of transfer functions normalized with the primordial curvature as

$$X(\mathbf{k}, \eta) = T_X(k, \eta) R_{\text{in}}(\mathbf{k}) . \quad (4.8)$$

Then, by computing the different contributions we find

$$\begin{aligned} \xi_{Q\alpha}^{\text{newt}} &\equiv \langle [b_Q \delta + \mathcal{H}^{-1} \partial_r(\mathbf{n} \cdot \mathbf{v})](\mathbf{n}, z_1) [b_\alpha \delta + b_v \mathcal{H}^{-1} \partial_r(\mathbf{n} \cdot \mathbf{v})](\mathbf{n}, z_2) \rangle \\ &= b_Q(z_1) b_\alpha(z_2) \int \frac{dk}{2\pi^2} k^2 T_\delta(k, \eta_1) T_\delta(k, \eta_2) P_R(k) j_0(kx) \\ &\quad + b_v(z_2) \int \frac{dk}{2\pi^2} \frac{k^4}{\mathcal{H}(z_1) \mathcal{H}(z_2)} T_v(k, \eta_1) T_v(k, \eta_2) P_R(k) \\ &\quad \times \left[\frac{1}{5} j_0(kx) - \frac{4}{7} j_2(kx) + \frac{8}{35} j_4(kx) \right] \\ &\quad + \int \frac{dk}{2\pi^2} k^3 P_R(k) \left[\frac{b_Q(z_1) b_v(z_2)}{\mathcal{H}(z_2)} T_\delta(k, \eta_1) T_v(k, \eta_2) + \frac{b_\alpha(z_2)}{\mathcal{H}(z_1)} T_v(k, \eta_1) T_\delta(k, \eta_2) \right] \\ &\quad \times \left[-\frac{1}{3} j_0(kx) + \frac{2}{3} j_2(kx) \right] \end{aligned} \quad (4.9)$$

where $x = x(z_1, z_2)$, and we allow for redshift dependent bias factors, while we have implicitly assumed that these are scale independent. Nevertheless a generalization to scale dependent bias factor would be straightforward. We define the correlation function induced by cosmic magnification as follows

$$\xi_{Q\alpha}^{\text{magnification}} \equiv \left\langle \left[\frac{5s-2}{2r} \int_0^r dr' \left[\frac{r-r'}{r'} \Delta_\Omega \right] (\Phi + \Psi) \right](\mathbf{n}, z_1) [b_\alpha \delta + b_v \mathcal{H}^{-1} \partial_r(\mathbf{n} \cdot \mathbf{v})](\mathbf{n}, z_2) \right\rangle . \quad (4.10)$$

Because of the integral along the line of sight this expression can not be written in a simple form like Eq. (4.9), unless we adopt Limber approximation [37]. We therefore prefer to compute explicitly this contribution through Eq. (4.3). We define the relativistic contribution as follows

$$\begin{aligned}\xi_{Q\alpha}^{\text{relativistic}} &\equiv \langle \Delta_Q(\mathbf{n}, z_1) \delta_F(\mathbf{n}, z_2) \rangle - \xi_{Q\alpha}^{\text{newt}} - \xi_{Q\alpha}^{\text{magnification}} \\ &\equiv \xi_{Q\alpha}^{\text{Doppler}} + \xi_{Q\alpha}^{\text{potential}} + \xi_{Q\alpha}^{\text{non-local}}\end{aligned}\quad (4.11)$$

where we have a Doppler term³

$$\begin{aligned}\xi_{Q\alpha}^{\text{Doppler}} &\equiv \langle [[b_Q \delta + \mathcal{H}^{-1} \partial_r(\mathbf{n} \cdot \mathbf{v}) + \mathcal{R}_Q \mathbf{n} \cdot \mathbf{v}] (\mathbf{n}, z_1) [b_\alpha \delta + b_v \mathcal{H}^{-1} \partial_r(\mathbf{n} \cdot \mathbf{v}) + \mathcal{R}_\alpha \mathbf{n} \cdot \mathbf{v}] (\mathbf{n}, z_2)] \\ &\quad - \xi_{Q\alpha}^{\text{newt}} \\ &= \int \frac{dk}{2\pi^2} k^2 P_R(k) j_1(kx) \\ &\quad [b_Q(z_1) \mathcal{R}_\alpha(z_2) T_\delta(k, \eta_1) T_v(k, \eta_2) - \mathcal{R}_Q(z_1) b_\alpha(z_2) T_v(k, \eta_1) T_\delta(k, \eta_2)] \\ &\quad + \int \frac{dk}{2\pi^2} k^3 P_R(k) \left[-\frac{3}{5} j_1(kx) + \frac{2}{5} j_3(kx) \right] \left[\frac{\mathcal{R}_\alpha(z_2)}{\mathcal{H}(z_1)} - \frac{\mathcal{R}_Q(z_1) b_v(z_2)}{\mathcal{H}(z_2)} \right] T_v(k, \eta_1) T_v(k, \eta_2) \\ &\quad + \int \frac{dk}{2\pi^2} k^2 P_R(k) \left[\frac{1}{3} j_0(kx) - \frac{2}{3} j_2(kx) \right] \mathcal{R}_Q(z_1) \mathcal{R}_\alpha(z_2) T_v(k, \eta_1) T_v(k, \eta_2)\end{aligned}\quad (4.12)$$

with

$$\mathcal{R}_Q = \frac{\dot{\mathcal{H}}}{\mathcal{H}^2} + \frac{2-5s}{r_S \mathcal{H}} + 5s - f_{\text{evo}}^Q, \quad (4.13)$$

$$\mathcal{R}_\alpha = b_R \left(3 + \frac{\dot{\mathcal{H}}}{\mathcal{H}^2} - f_{\text{evo}}^{\text{Ly}\alpha} \right), \quad (4.14)$$

where we use a biased expression for \mathcal{R}_α . And the potential term is

$$\begin{aligned}\xi_{Q\alpha}^{\text{potential}} &\equiv \langle [[b_Q \delta + \mathcal{H}^{-1} \partial_r(\mathbf{n} \cdot \mathbf{v}) + \mathcal{R}_Q \mathbf{n} \cdot \mathbf{v} + \mathcal{P}_Q] (\mathbf{n}, z_1) [b_\alpha \delta + b_v \mathcal{H}^{-1} \partial_r(\mathbf{n} \cdot \mathbf{v}) + \mathcal{R}_\alpha \mathbf{n} \cdot \mathbf{v} + \mathcal{P}_\alpha] (\mathbf{n}, z_2)] \\ &\quad - \xi_{Q\alpha}^{\text{newt}} - \xi_{Q\alpha}^{\text{Doppler}} \\ &= \int \frac{dk}{2\pi^2} k^2 P_R(k) j_0(kx) [b_Q(z_1) T_\delta(k, \eta_1) T_{\mathcal{P}_\alpha}(k, \eta_2) + b_\alpha(z_2) T_{\mathcal{P}_Q}(k, \eta_1) T_\delta(k, \eta_2)] \\ &\quad + \int \frac{dk}{2\pi^2} k^3 P_R(k) \left[-\frac{1}{3} j_0(kx) + \frac{2}{3} j_2(kx) \right] \\ &\quad \left[\frac{1}{\mathcal{H}(z_1)} T_v(k, \eta_1) T_{\mathcal{P}_\alpha}(k, \eta_2) + \frac{b_v(z_2)}{\mathcal{H}(z_2)} T_{\mathcal{P}_Q}(k, \eta_1) T_v(k, \eta_2) \right] \\ &\quad + \int \frac{dk}{2\pi^2} k^2 P_R(k) j_1(kx) [\mathcal{R}_Q(z_1) T_v(k, \eta_1) T_{\mathcal{P}_\alpha}(k, \eta_2) - \mathcal{R}_\alpha(z_2) T_{\mathcal{P}_Q}(k, \eta_1) T_v(k, \eta_2)] \\ &\quad + \int \frac{dk}{2\pi^2} k^2 P_R(k) j_0(kx) T_{\mathcal{P}_Q}(k, \eta_1) T_{\mathcal{P}_\alpha}(k, \eta_2)\end{aligned}\quad (4.15)$$

³For the velocity transfer function $T_v(k, \eta)$ we follow the notation of Ref. [25, 38], namely it refers to vector potential V defined through $\mathbf{v} = i\mathbf{k}V$.

where we have used the following definitions

$$\mathcal{P}_Q = (5s - 2)\Phi + \left(1 + \frac{\dot{\mathcal{H}}}{\mathcal{H}^2} + \frac{2 - 5s}{r_S \mathcal{H}} + 5s - f_{\text{evo}}^Q\right)\Psi + \mathcal{H}^{-1}\dot{\Phi} + (f_{\text{evo}}^Q - 3)\mathcal{H}v, \quad (4.16)$$

$$\mathcal{P}_\alpha = b_R \left[\left(3 + \frac{\dot{\mathcal{H}}}{\mathcal{H}^2} - f_{\text{evo}}^{\text{Ly}\alpha}\right)\Psi + \mathcal{H}^{-1}\dot{\Phi} + (f_{\text{evo}}^{\text{Ly}\alpha} - 3)\mathcal{H}v \right], \quad (4.17)$$

and $T_{\mathcal{P}_Q}$ and $T_{\mathcal{P}_\alpha}$ denote the respective transfer functions normalized with the primordial curvature perturbation. The last term in Eq. (4.11) denotes the contribution of the non-local terms, and their cross-correlation with all the other terms. In particular this includes the correlation between QSO magnification with all (local and non-local) Lyman- α relativistic effects and the correlation between relativistic non-local terms (e.g. ISW, Shapiro time delay) with everything else. Again, as we did for the cosmic magnification we prefer to use Eq. (4.3) to compute them.

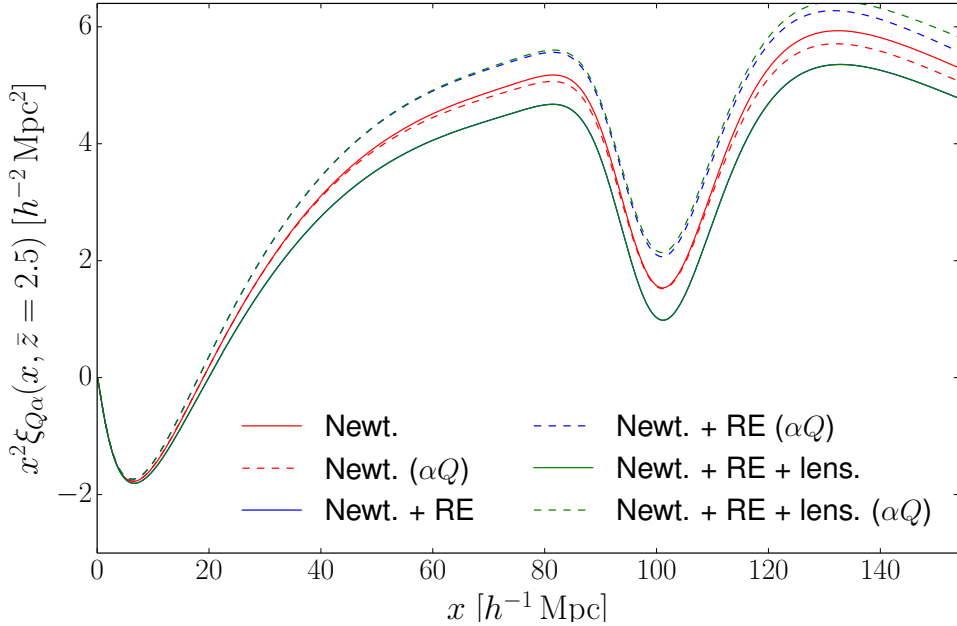


Figure 2. The figure shows the Quasar-Lyman- α cross-correlation function, along the line of sight. Different colours correspond to different contributions: red - Newtonian terms (Newt.), blue - Newtonian and relativistic effects (RE), green - Newtonian, relativistic and lensing terms. The full line and dashed line correspond to the cross-correlations $\xi_{Q\alpha}$ and $\xi_{\alpha Q}$ respectively. The asymmetry due to the bias evolution, relativistic effects and lensing produce a split of the cross-correlation function around the symmetric part. The dominant effect due to the peculiar velocities of the tracers (Doppler effect) is large on all scales above $20 h^{-1} \text{ Mpc}$ while the lensing and redshift evolution effects grow significantly towards larger scales.

Fig. 2 shows different contributions to the overall cross-correlation function. The red line shows the contribution from the Newtonian terms ($\xi_{\alpha Q}^{\text{Newt}}$), which are the most standard ones considered in the large-scale correlation analysis. The largest correction to the signal comes from the relativistic effects ($\xi_{\alpha Q}^{\text{RE}}$), more specifically from the Doppler terms (see the subsection on anti-symmetric part for details). The signal from the relativistic effects is nearly constant for all scales above $\sim 40 h^{-1}\text{Mpc}$, and is of around 10% compared to the pure Newtonian terms. Further we show that the lensing contribution only gives a small correction at large scales. Dashed lines correspond to the cross-correlation $\xi_{\alpha Q}$, where the positions of Lyman- α and QSO have been exchanged (see Fig. 1). This exchange is equivalent to the transformation $x \rightarrow -x$.

The correction due to relativistic effects is much larger than anticipated from the galaxy surveys, which is due to two effects: firstly, the difference in biases is much larger for QSO and Lyman- α tracers than for two galaxy populations, and secondly, the overall signal from the Newtonian terms is larger as well. The calculations for two galaxy populations have already been shown in [18].

4.1 Local term expansion in \mathcal{H}/k

In our derivation we have been as general as possible and our results are valid for any metric theory of gravity provided that photons move along geodesic and photon number is conserved. Since we describe geometrically our observable, the theory of gravity can modify the transfer functions only⁴, as long as the previous assumptions are valid. We have also assumed that sources move along geodesics, but this assumption can be easily relieved. In order to give the flavor of the amplitude in different regimes of the effects previously computed in a relativistic framework, we replace the transfer functions with their counterparts in a 'newtonian' framework. This oversimplification will give us the physical understanding of the effects shown in the next sections. Therefore, we apply the following substitutions

$$T_v(k, \eta) \rightarrow -\frac{\mathcal{H}}{k} f T_\delta(k, \eta) \quad (4.18)$$

$$T_\Psi(k, \eta) \rightarrow -\frac{3}{2} \frac{\mathcal{H}^2}{k^2} \Omega_M T_\delta(k, \eta) \quad (4.19)$$

$$T_\Phi(k, \eta) \rightarrow -\frac{3}{2} \frac{\mathcal{H}^2}{k^2} \Omega_M T_\delta(k, \eta) \quad (4.20)$$

$$T_{\dot{\Phi}}(k, \eta) \rightarrow -\frac{3}{2} \frac{\mathcal{H}^3}{k^2} \Omega_M (f - 1) T_\delta(k, \eta) \quad (4.21)$$

where the growth factor can be approximated in perturbation theory in ΛCDM by $f(z) = \Omega_M(z)^{0.6}$.

By evaluating all the cosmological parameters and biases at the mean redshift z_{mean}

⁴We remark that expressions for bias factors implicitly assume a theory of gravity.

we find

$$\begin{aligned}\xi_{Q\alpha}^{\text{newt}} &\sim b_Q b_\alpha \int \frac{dk}{2\pi^2} k^2 P(k) j_0(kx) \\ &\quad + b_v \int \frac{dk}{2\pi^2} k^2 f^2 P(k) \left[\frac{1}{5} j_0(kx) - \frac{4}{7} j_2(kx) + \frac{8}{35} j_4(kx) \right] \\ &\quad + (b_Q b_v + b_\alpha) \int \frac{dk}{2\pi^2} k^2 f P(k) \left[\frac{1}{3} j_0(kx) - \frac{2}{3} j_2(kx) \right],\end{aligned}\quad (4.22)$$

$$\begin{aligned}\xi_{Q\alpha}^{\text{Doppler}} &\sim (-b_Q \mathcal{R}_\alpha + \mathcal{R}_Q b_\alpha) \int \frac{dk}{2\pi^2} k^2 f P(k) j_1(kx) \frac{\mathcal{H}}{k} \\ &\quad + (-\mathcal{R}_\alpha + \mathcal{R}_Q b_v) \int \frac{dk}{2\pi^2} k^2 f^2 P(k) \left[\frac{3}{5} j_1(kx) - \frac{2}{5} j_3(kx) \right] \frac{\mathcal{H}}{k} \\ &\quad + \mathcal{R}_\alpha \mathcal{R}_Q \int \frac{dk}{2\pi^2} k^2 f^2 P(k) \left[\frac{1}{3} j_0(kx) - \frac{2}{3} j_2(kx) \right] \left(\frac{\mathcal{H}}{k} \right)^2,\end{aligned}\quad (4.23)$$

$$\begin{aligned}\xi_{Q\alpha}^{\text{potentials}} &\sim (b_Q \tilde{\mathcal{P}}_\alpha + \tilde{\mathcal{P}}_Q b_\alpha) \int \frac{dk}{2\pi^2} k^2 P(k) j_0(kx) \left(\frac{\mathcal{H}}{k} \right)^2 \\ &\quad + (\tilde{\mathcal{P}}_\alpha + \tilde{\mathcal{P}}_Q b_v) \int \frac{dk}{2\pi^2} k^2 f P(k) \left[\frac{1}{3} j_0(kx) - \frac{2}{3} j_2(kx) \right] \left(\frac{\mathcal{H}}{k} \right)^2 \\ &\quad + (-\mathcal{R}_Q \tilde{\mathcal{P}}_\alpha + \tilde{\mathcal{P}}_Q \mathcal{R}_\alpha) \int \frac{dk}{2\pi^2} k^2 f P(k) j_1(kx) \left(\frac{\mathcal{H}}{k} \right)^3 \\ &\quad + \tilde{\mathcal{P}}_\alpha \tilde{\mathcal{P}}_Q \int \frac{dk}{2\pi^2} k^2 P(k) j_0(kx) \left(\frac{\mathcal{H}}{k} \right)^4\end{aligned}\quad (4.24)$$

where $P(k) = T_\delta(k, \eta)^2 P_R(k)$ denotes the matter power spectrum at the mean redshift. $\tilde{\mathcal{P}}_Q$ and $\tilde{\mathcal{P}}_\alpha$ are the pre-factors defined through the transformations (4.18 - 4.21), namely

$$T_{\mathcal{P}_Q}(k, \eta) \rightarrow \tilde{\mathcal{P}}_Q \frac{\mathcal{H}^2}{k^2} T_\delta(k, \eta), \quad (4.25)$$

$$T_{\mathcal{P}_\alpha}(k, \eta) \rightarrow \tilde{\mathcal{P}}_\alpha \frac{\mathcal{H}^2}{k^2} T_\delta(k, \eta), \quad (4.26)$$

and they can be explicitly computed

$$\tilde{\mathcal{P}}_Q = \frac{3}{2} \Omega_M \left(2 - f + f_{\text{evo}}^Q - \frac{\dot{\mathcal{H}}}{\mathcal{H}^2} + \frac{2f}{3\Omega_M} (3 - f_{\text{evo}}^Q) - 10s + \frac{5s - 2}{\mathcal{H}r} \right), \quad (4.27)$$

$$\tilde{\mathcal{P}}_\alpha = b_R \frac{3}{2} \Omega_M \left(-2 + f_{\text{evo}}^{\text{Ly}\alpha} - \frac{\dot{\mathcal{H}}}{\mathcal{H}^2} - f + \frac{2f}{3\Omega_M} (3 - f_{\text{evo}}^{\text{Ly}\alpha}) \right). \quad (4.28)$$

We remark that the transformation (4.18 - 4.21) has been performed by using Newtonian equations. Nevertheless, it is well known that, for CDM, linearized Einstein equations agree with Newtonian dynamics if perturbations are considered in specific gauges, namely the density perturbation in synchronous gauge and the velocity in Newtonian gauge. Since we have chosen to express perturbations in this combination of

gauges, the expressions here derived include correctly the GR dynamics, as long as the approximation that CDM is the only species which contributes to perturbations is valid.

According to this scheme, we note that all the newtonian terms contribute at the same parametrical order. The Doppler term, Eq. (4.23), contains the leading correction of order \mathcal{H}/k to the newtonian approximation. This term is non-vanishing only if we use two different tracers or probes. With a single tracer the leading correction would be of the order $(\mathcal{H}/k)^2$, and the amplitude of these terms would be much more suppressed. The leading corrections have also a different parity under the exchange $x \leftrightarrow -x$. Because of that, they contribute only to the antisymmetric part of the correlation function, while newtonian terms (with biases and cosmology evaluated at the mean redshift z_{mean}) lead to a symmetric correlation function only. This argument does not only show the importance of using different probes to try to measure relativistic correction, as already shown in [13, 14, 16, 18], but it also indicates that when we consider cross-correlations between different probes we need to carefully consider effects which might be neglected with a single tracer, as shown in [14, 19]. For simplicity, in this counting scheme we did not include integrated effects like cosmic magnification, ISW and Shapiro time delay effects. It is known that cosmic magnification can be of the same parametrical order of density and redshift space distortion perturbations, see e.g. [17, 39, 40] and we do include it in the full relativistic analysis in next sections. In the full analysis there is also a contribution to the antisymmetric correlation function due to newtonian terms because of the biases and cosmological parameter evolutions, that have been neglected in this simple approach.

4.2 Symmetric correlation function

The correlation function (4.1) can decompose in a symmetric and anti-symmetric part. In this section we are interested in the symmetric correlation function

$$\xi_{(Q\alpha)}(z_1, z_2, \theta) = \frac{\xi_{Q\alpha}(z_1, z_2, \theta) + \xi_{\alpha Q}(z_1, z_2, \theta)}{2} \quad (4.29)$$

Up to the redshift dependence of transfer functions or bias factors, only the correlation functions which involve even spherical Bessel functions contribute to the symmetric part of the correlation function.

Figure 3 shows the symmetric contribution to the QSO-Lyman- α cross-correlation function. As expected the Newtonian terms (density and RSD) dominate the symmetric signal, while the Relativistic terms (Doppler and potential) only slightly contaminate the result. Similar effect could be observed when one considers only auto-correlations of one tracer. It is interesting to note that while both the Doppler and potential terms in the symmetric form are of the same order of magnitude in the expansion of k ($\sim (\mathcal{H}/k)^2$), the values of the cosmological and bias prefactors are different - mainly the large contribution to the Doppler term comes from the large values of the QSO (f_{evo}^Q) and Lyman- α evolution bias ($f_{\text{evo}}^{\text{Ly}\alpha}$). Also, while Doppler terms are in general larger than the potential terms, the later become the leading sub-dominant signal at small scales. At very large scales, on the other hand, the lensing terms of the QSO start to become

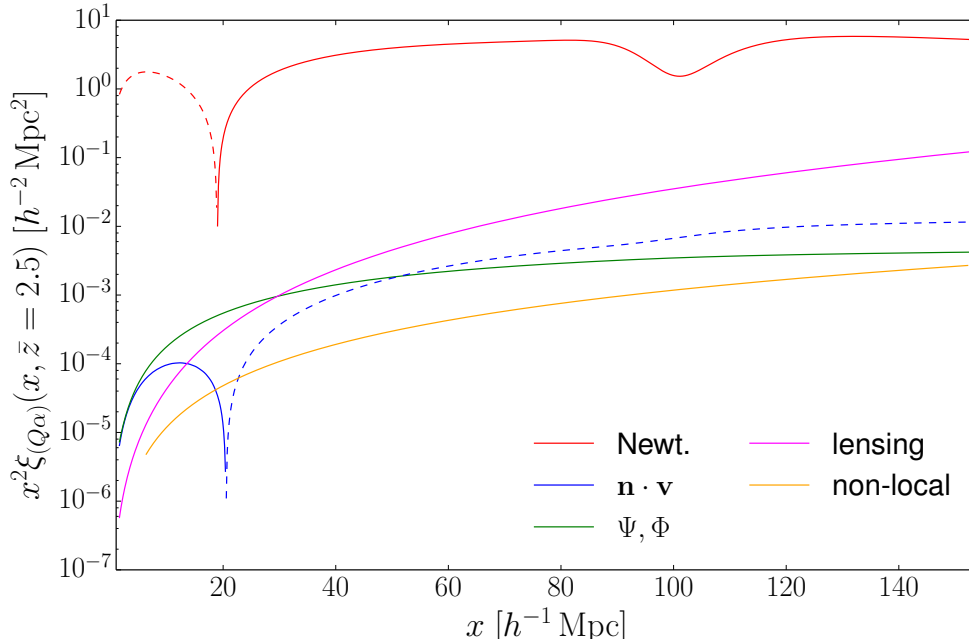


Figure 3. The figure shows the symmetric part of the Quasar-Lyman- α cross-correlation function, along the line of sight. Different colours correspond to different contributions: red - Newtonian terms (Newt.), blue - Doppler terms, green - potential terms, magenta - lensing terms and orange - non-local terms. The full line and dashed line correspond to the positive and negative values of the cross-correlations respectively. Newtonian terms dominate the signal in the symmetric part of the cross-correlation function. Note that non-local terms were not computed at very small scales due to numerical issues, however they are very small. The lensing contribution (magenta) is increasing towards large scales which has been subject to many discussions in the literature (see text for details).

the dominant contaminant. This is the main idea behind the recent papers claiming that using a large window function in the radial direction will boost the lensing signal [17]. In fact, it is more about decreasing the overall signal of the density perturbation, which remain more or less constant in radial direction, compared to the lensing term which is always increasing with the distance.

The non-local terms are always small compared to the other effects in the symmetric part of the cross-correlation function. As for the lensing part of the non-local terms, the relative contribution of it grows for large (redshift) separations.

4.3 Anti-symmetric correlation function

Analogously to the symmetric part, we can define the anti-symmetric part of the correlation function

$$\xi_{[Q\alpha]}(z_1, z_2, \theta) = \frac{\xi_{Q\alpha}(z_1, z_2, \theta) - \xi_{\alpha Q}(z_1, z_2, \theta)}{2}. \quad (4.30)$$

A non vanishing anti-symmetric correlation function will indicate a violation of the exchange symmetry of the tracers ($z_1 \leftrightarrow z_2$). Thus, the interchange of the tracers at the same position would produce different results, and which tracer is in the background and which in the foreground would matter. However, this is only true when one is dealing with differently biased tracers. If, for instance, one computes the auto-correlation function of one single tracer, the correlation function will be by definition symmetric. On the other hand two different effects can break the symmetry when dealing with different tracers. The asymmetry can come either from different value and redshift evolution of the bias factors or from the intrinsic evolution of the transfer functions. In the case of the galaxy surveys that is the case, and several sources of the asymmetry have been identified and suggested in the literature (e.g. gravitational redshift, Doppler effects, etc.) [13, 16, 18]. These effects reflect the fact that there is not a translation symmetry along the redshift direction, and the asymmetry is generated along the radial direction. Whereas in the angular direction, if statistical isotropy and (angular) homogeneity are not broken, any asymmetry can not be sourced.

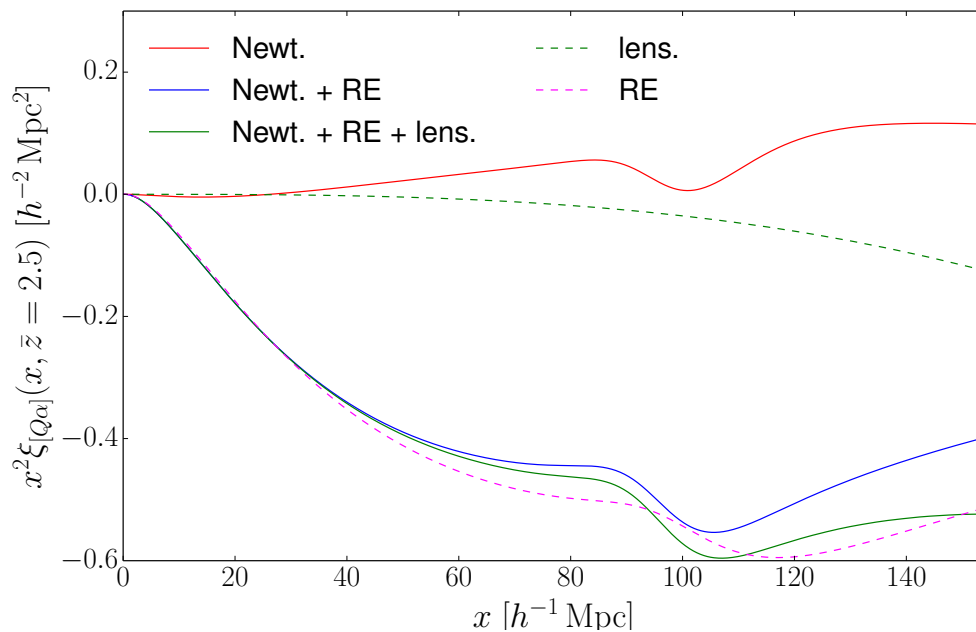


Figure 4. The figure shows different contributions to the anti-symmetric part of the cross-correlation function, along the line of sight. Full red line shows the contribution due to the often neglected redshift evolution of the bias factors, dashed magenta line shows the contribution due to the relativistic effects and dashed green line contribution of the lensing terms. The full blue and green lines represent summing up various different terms - redshift evolution and Doppler terms (full blue line), and all the effects (full green line). The main contributor to the signal are the relativistic effects (mostly Doppler terms), while the bias redshift evolution and lensing form the sub-dominant corrections of order of 10% of the signal in the anti-symmetric cross-correlations.

Our calculations in the previous sections show that the main source of asymmetry of the correlation functions comes from the Doppler terms in the relativistic expansion (see Fig. 4). In our simple expansion, see Eqs. (4.22, 4.23, 4.24), the Doppler term, Eq. (4.23) contains terms with odd spherical Bessel functions multiplied by only one factor \mathcal{H}/k . In the Newtonian term, Eq. (4.22), all the terms are multiplied by even Bessel function, and the asymmetry is generated by the redshift dependence only, while in potential term, Eq. (4.24), the terms with odd Bessel function are suppressed by $(\mathcal{H}/k)^3$. The largest single contribution is the Doppler - density correlation which is boosted by the difference in bias factors (see Eq. 4.23). This result is known in the literature and has been commented on at various times, mostly in the context of two galaxy populations [13, 18]. In this paper we have focused on two tracers whose bias factors are as different as possible: quasar bias being very large, and Lyman- α forest flux bias being even negative. Thus ensuring that the signal from the Doppler effect is boosted as much as possible.

The first of the sub-dominant signals is the redshift evolution of the bias factors (see Fig. 4). Usually one approximates the redshift dependent quantities within a redshift bin with a constant value at the mean redshift. However, redshift evolution of the bias factors gives a fairly large contribution to the asymmetry. This contribution mainly comes from the standard Kaiser terms - indeed one can easily replicate the results by using well known Eq. (4.22) and requiring that the bias factors for quasar and Lyman- α are evaluated not at the mean redshift z_{mean} but at z_1 and z_2 respectively. Strictly speaking, this effect should not be considered for biases only, but for any redshift dependent prefactors (e.g. cosmological prefactors of the relativistic effects, growth factors, etc.), however in our calculations the effects of growth of structure and evolution of the cosmological parameters (most notably $H(z)$) are very small compared to the other effects, and are well below the 1% of the final result. Thus one can safely use the approximation of constant cosmological parameters evaluated at the mean redshift.

The signal of the bias redshift evolution gives an important contribution, that needs to be modeled if one wants to measure the effects to below 10% accuracy. While it can be regarded as a nuisance signal to the relativistic effects, it requires a precise knowledge of the bias redshift dependence of both tracers. However, this information can be acquired from independent and complementary results, such as auto-correlation functions of each of the tracers, and can be well constrained.

Fig. 5 shows the contributions of the relativistic terms to the anti-symmetric part of the $\xi_{Q\alpha}$, broken down into its components. It is clear that at all scales the cross-correlations due to Doppler terms dominate the relativistic signal, while the potential and non-local parts are small. The next to leading order corrections in the anti-symmetric part come from the redshift evolution of the bias factors in the Newtonian terms, an effect often considered to be too small to be of any importance. In the case of QSO-Lyman- α cross-correlation it is an important sub-dominant contribution to the anti-symmetric part. Compared to the symmetric part of the $\xi_{Q\alpha}$ (see Fig. 3) the potential terms are also suppressed at all scales, even compared to the non-local terms.

A special note deserves the fact that all the contaminating effects are small at the

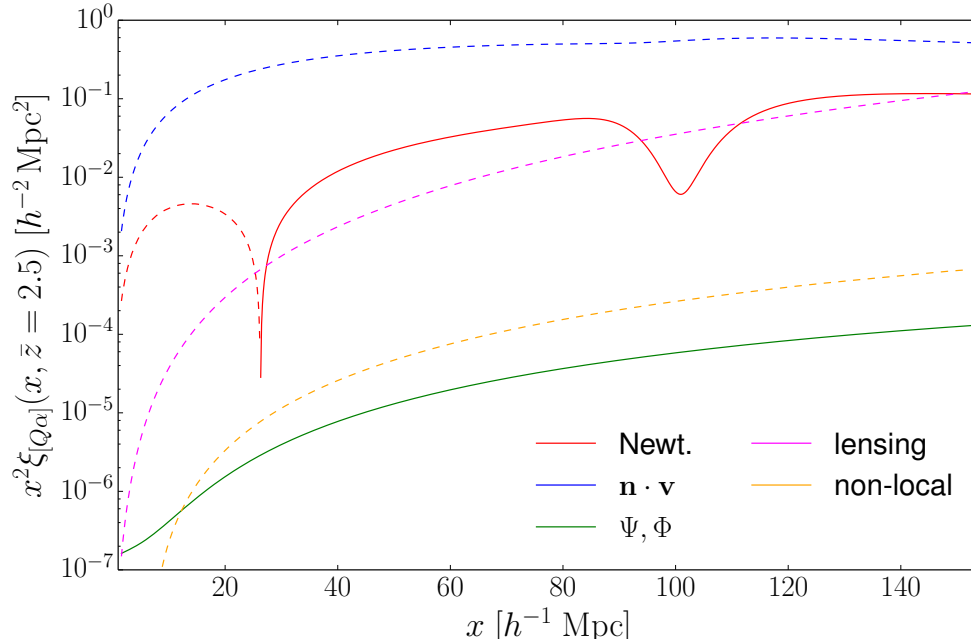


Figure 5. The figure shows different contributions to the relativistic effects in anti-symmetric part of the cross-correlation function, along the line of sight. The blue line shows contributions due to the Doppler effects, red line due to potential terms, and green line due to all non-local terms. The difference between full and dashed line is whether the contribution to $\xi_{[Q\alpha]}$ is positive or negative respectively. Compared to the symmetric part the potential and Newtonian terms are strongly suppressed.

BAO scale. This result does not carry any deeper significance, and is a result of the values of bias factors for the tracers used in this study. Nevertheless, for this particular case it does allow for an easier estimation of the relativistic effects at the BAO scale - which is already a target of many surveys and being a robust feature, very accurately measured.

Figure 6 shows that the signal of the relativistic effects is largest at the BAO scale, compared to the cross-correlation function computed just with Newtonian terms. The size of the asymmetry is around 10%. One should note that even though the ratio reach around 30% at the BAO scale this is an artificial enhancement of the signal since the cross-correlation function drops nearly to zero. The relativistic effects are nearly constant on the scale larger than $\sim 40 h^{-1}\text{Mpc}$ and contribute to around 10% distortion on all scales larger than that.

The second contaminating effect is that of the weak lensing signal of quasars. In our specific case the lensing signal can be as large as the effects due to the bias redshift evolution. Similarly to the bias redshift evolution signal, the lensing signal becomes more important on larger scales, and requires careful modeling if one is to measure the overall asymmetry effects to a high precision.

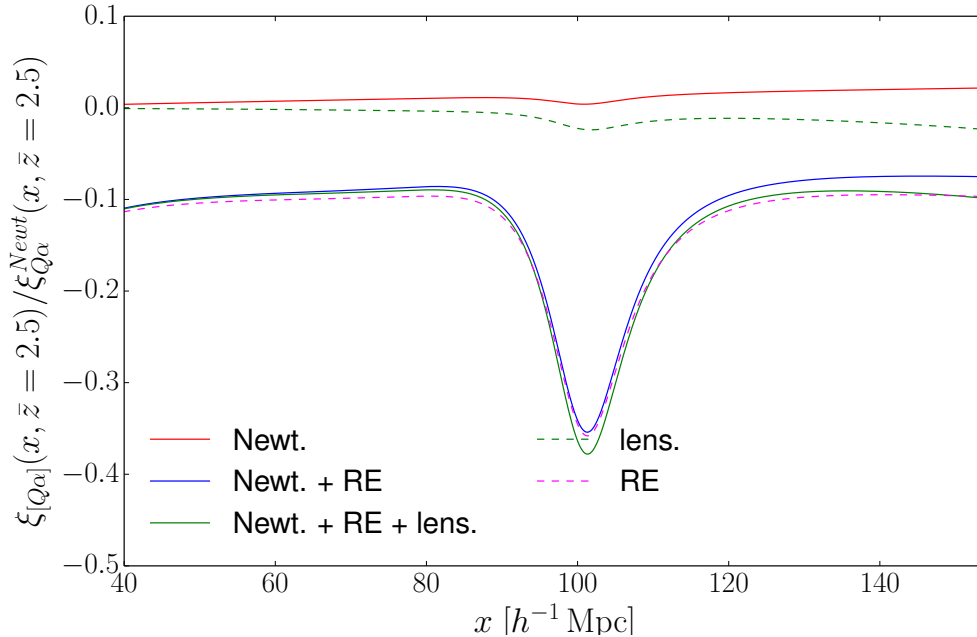


Figure 6. The figure shows the relative size of the anti-symmetric part of the cross-correlation function, along the line of sight, for different terms. Full red line shows the contribution due to the redshift evolution of the bias factors, dashed magenta line shows the contribution due to the relativistic effects and dashed green line contribution of the lensing terms. The full blue and green lines represent summing up various different terms - redshift evolution and Doppler terms (full blue line), and all the effects (full green line). The relativistic effects can be as large as 10% at all scales above $\sim 40 h^{-1}\text{Mpc}$, compared to the pure Newtonian calculation (including the bias redshift evolution).

However, the weak lensing effect is proportional to the magnification bias (and on density bias, since the leading term is $\langle \kappa \delta \rangle$), and thus its signal is strongly dependent on this nuisance parameter. We caution that magnification bias needs to be well known, and possibly constrained from independent results, to avoid the contamination of the signal. The imprecise knowledge of the bias factor affects larger scales the most, it remains important contaminant even at the BAO scales, where it affects the amplitude of the BAO peak, but not its position. Figure 7 shows the effects on the asymmetry produced if we change the measured parameters of the Quasar Luminosity Function used to derive the evolution and magnification bias parameters. While the effect of the evolution bias parameter is smaller, it is also degenerate with the effect of the magnification bias at larger scales. However, the change of parameters by 5% shown in the plot is conservative, and future surveys and current surveys will be able to estimate the quasar luminosity function more accurately and hence provide a better estimate on the parameter f_{evo}^Q .

In a standard (single tracer) large scale observable, relativistic effects (except cos-

mic magnification) are naively suppressed on sub-Hubble scales by the variance induced by the leading newtonian terms and are limited by cosmic variance on large scales. Because of these limitations, all forecasts, see e.g. [14, 15, 19], predict that they are not observable in current and future planned surveys. Nevertheless the antisymmetric correlation function, and more generically the dipole of the 2-point function, represents an independent observable whose leading signal is determined, as we have shown, by relativistic corrections. Hence the detection of relativistic effects is not anymore limited by cosmic variance but it becomes a shot-noise limited observable. Therefore, relativistic effects can be detected on scale much smaller than Hubble size. Not only larger scale experiment, but also advanced data analysis technique like multi-tracers [41], shot-noise canceling [42] and generically correlations between different tracers will probably require to include relativistic effects to correctly interpret the observation and to avoid to introduce any theoretical bias.

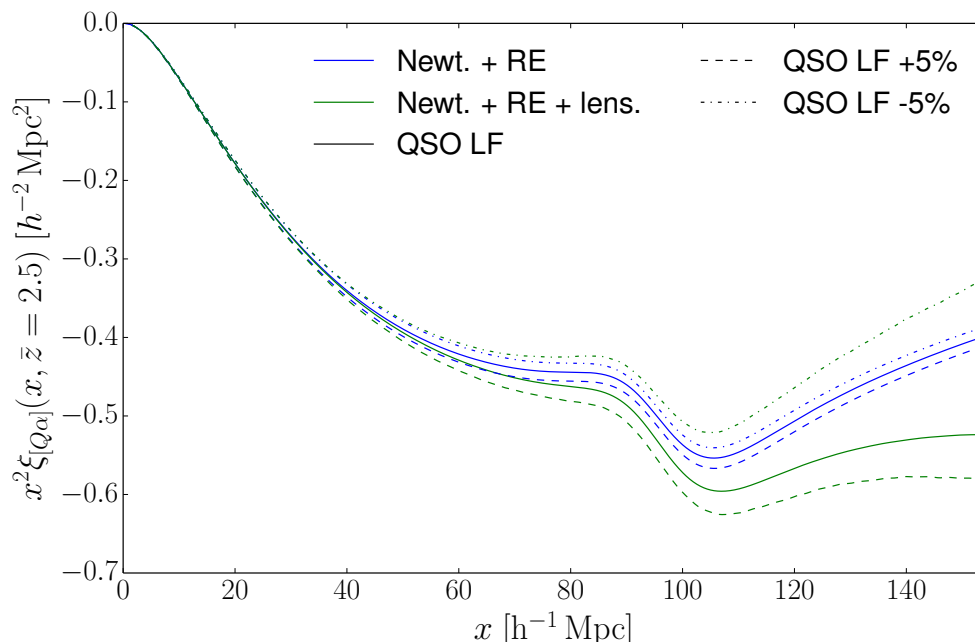


Figure 7. The asymmetry part of the QSO-Lyman- α cross-correlation function, along the line of sight. Blue colour represents Newtonian and relativistic terms, while green colour adds lensing to them. The different line shapes correspond to different values of the bias parameters: full line shows the mean values used in our calculations, dashed line shows the values ($s = 0.256883$, $f_{\text{evo}}^Q = 6.19163$) for +5% change to the QSO LF parameters and dot-dashed the values ($s = 0.450115$, $f_{\text{evo}}^Q = 4.74261$) for -5% change to the QSO LF parameters. Even at the BAO scales - the values of the evolution and magnification bias can affect the result by 10% and need to be modeled carefully.

The last effect that can potentially contaminate the cosmological signal in the relativistic terms is the uncertainty in the $f_{\text{evo}}^{\text{Ly}\alpha}$. Its exact value depends on the assumption

about the redshift evolution of the mean gas temperature and the ionizing UV background.

Arguably one might worry that such a redshift evolution will change the value of $f_{\text{evo}}^{\text{Ly}\alpha}$. While that is in principle true, the change is not significant.

The current measurements of the UV background evolution ([43]) suggest that $\Gamma_{\gamma,HI}$ is a constant in the redshift range of $z = 2 - 4$. While both the semi-analytical models and numerical simulations suggest an evolving $\Gamma_{\gamma,HI}$, the predicted redshift evolution is decreasing with redshift in the redshift range in question, and is consistent with the measurements. A decreasing redshift evolution in the UV background would further decrease $f_{\text{evo}}^{\text{Ly}\alpha}$, resulting in stronger overall signal in the asymmetric part of the cross-correlation function (see the corresponding +5% line in Fig. 8).

On the other hand the measurements of the mean temperature show that it is increasing with redshift at $z = 2 - 3$ [44]. Thus the evolution of T_0 would increase the value of $f_{\text{evo}}^{\text{Ly}\alpha}$ and decrease the signal of (primarily) Doppler term (see the corresponding -5% line in Fig. 8).

In principle the models and observations suggest a stronger evolution in the mean temperature which could lower $f_{\text{evo}}^{\text{Ly}\alpha}$, but the current estimates ([43, 44]) suggest that the true value is within $\pm 5\%$ of the value used in this paper ($f_{\text{evo}}^{\text{Ly}\alpha} = -3$).

4.4 Signal-to-noise analysis

We have performed a simple signal-to-noise analysis to show the relevance of the relativistic effects in the future surveys. We chose to follow a prescription in the Fourier space, used in [13]. While we note that our results and calculations have been done in real space, the Fourier space S/N calculation is still valid. Indeed, as long as we neglect systematic effects, if we cannot observe the effect in Fourier space, we cannot observe it in the real-space, and vice versa.

For the purpose of this calculation we have considered only the largest relativistic correction (Doppler effect) as the source of the new signal. We have shown that in our case this is a good approximation, moreover, it is the result of cutting the expansion in \mathcal{H}/k at second order. Thus the power spectra for the Lyman- α forest and QSO simplify to the well known Kaiser formula

$$\begin{aligned} P_{\alpha}(k, \mu) &= (b_{\alpha} + b_v \mu^2 f)^2 P(k) + \mathcal{O}(\mathcal{H}^2/k^2) \\ P_Q(k, \mu) &= (b_Q + \mu^2 f)^2 P(k) + \mathcal{O}(\mathcal{H}^2/k^2), \end{aligned} \quad (4.31)$$

where the angle follows the notation of this paper ($\mu \equiv -\mathbf{n} \cdot \hat{\mathbf{k}}$).

The cross-power can be obtained by combining Eqs. (3.17) and (3.25), dropping all terms of order \mathcal{H}^2/k^2 or higher and performing a Fourier transform. The result can be written as

$$P_{\alpha Q}(k, \mu) = \left(b_{\alpha} + b_v \mu^2 f + i \mathcal{R}_{\alpha} \mu \frac{\mathcal{H}}{k} \right) \left(b_Q + \mu^2 f - i \mathcal{R}_Q \mu \frac{\mathcal{H}}{k} \right) P(k), \quad (4.32)$$

where \mathcal{R}_Q and \mathcal{R}_{α} are given by Eq. (4.13) and (4.14) respectively. The values at $z = 2.5$ for these two terms are $\mathcal{R}_Q(z = 2.5) \approx -4.4$ and $\mathcal{R}_{\alpha} \approx -1.17$. The largest contribution comes from the evolution bias for both QSOs and Lyman- α forest. However, an

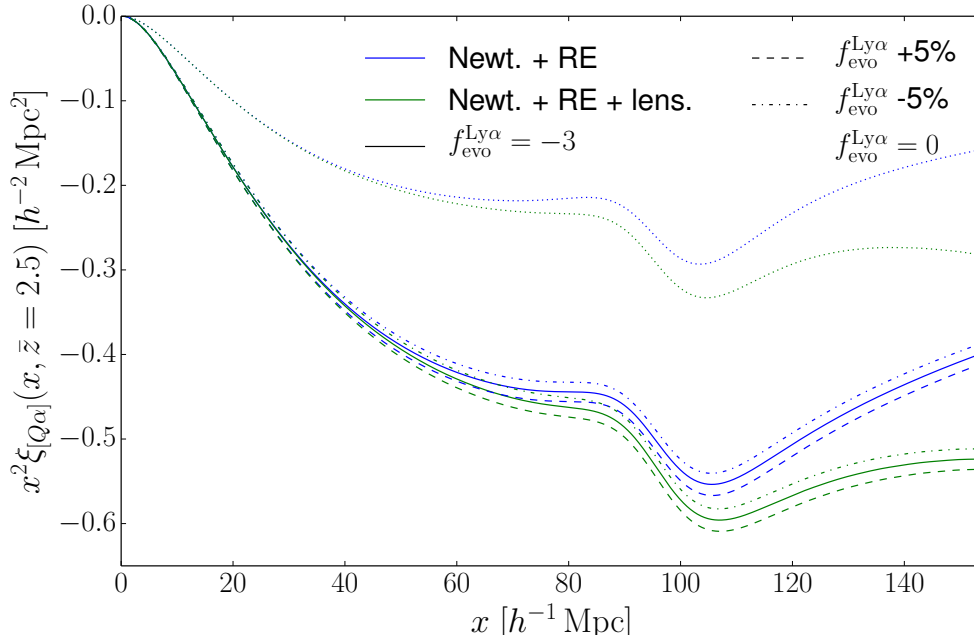


Figure 8. The asymmetry part of the QSO-Lyman- α cross-correlation function along the line of sight. Blue colour represents Newtonian and relativistic terms, while green colour adds lensing to them. The different line shapes correspond to different values of the Lyman- α evolution bias parameters: full line shows the mean values used in our calculations, dashed line shows the values ($f_{\text{evo}}^{\text{Ly}\alpha} = -3.15$) for +5% change to value adopted in this paper and dot-dashed the values ($f_{\text{evo}}^{\text{Ly}\alpha} = -2.85$) for -5% change to the mean value. The changes in the $\pm 5\%$ are very small, and seem to be in agreement with measured redshift evolutions ([43, 44]). The dotted line corresponds to a zero evolution bias, which is a very extreme case and would require a strong, increasing evolution in the mean temperature with redshift, and no evolution of the UV background.

important role is also played by the bias factor of relativistic terms (b_R), which lowers the value of \mathcal{R}_α and makes both terms of the same sign.

We have shown that the relativistic signals dominantly show in the anti-symmetric part of the cross-correlation function. Translating this effect to the Fourier space, it corresponds to the imaginary part of the cross power spectrum [13]. Splitting the cross power into the relevant contributions we define the real and imaginary part as

$$\begin{aligned}
 P_{\alpha Q}^R(k, \mu) &= (b_\alpha + b_v \mu^2 f) (b_Q + \mu^2 f) P(k) \\
 P_{\alpha Q}^I(k, \mu) &= \frac{\mathcal{H}}{k} \mu f [\mathcal{R}_\alpha (b_Q + \mu^2 f) - (b_\alpha + b_v \mu^2 f) \mathcal{R}_Q] P(k).
 \end{aligned}
 \tag{4.33}$$

The variance of the imaginary part, as shown by [13], is

$$\sigma_I^2(k, \mu) = P_{\alpha Q}^I{}^2 + \frac{1}{2} N_\alpha P_Q + \frac{1}{2} N_Q P_\alpha + \frac{1}{2} N_\alpha N_Q,
 \tag{4.34}$$

where N_α and N_Q are the noise power spectra for Lyman- α forest and QSOs respectively. The signal-to-noise estimator for a survey of a volume V is an integral over the modes of the per mode $(S/N)_k$ ratio:

$$\left(\frac{S}{N}\right)^2 = \frac{V}{8\pi^2} \int_{k_{\min}}^{k_{\max}} dk k^2 \int_{-1}^1 d\mu \left(\frac{P_{\alpha Q}^I(k, \mu)}{\sigma_I(k, \mu)} \right)^2, \quad (4.35)$$

where the large scale mode k_{\min} is determined by the volume of the survey, i.e. $k_{\min} \sim 2\pi/V^{1/3}$.

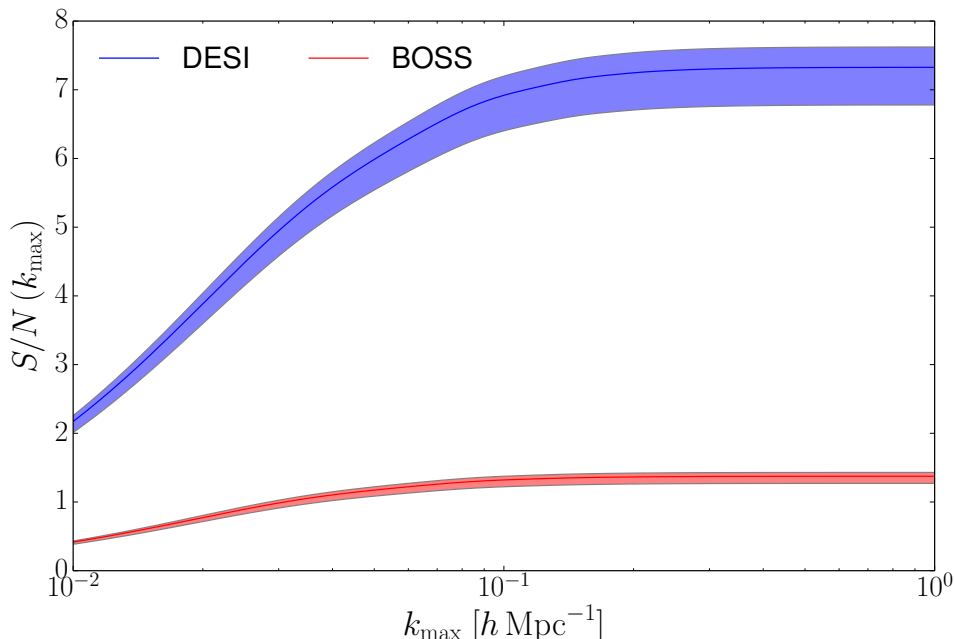


Figure 9. The plot shows the signal-to-noise ratio of the imaginary part of the QSO-Lyman- α cross-power for two different surveys: BOSS (in red) and DESI (in blue). The shaded regions for each survey show variability in the S/N ratio due to uncertainties in evolution/magnification biases for both QSOs and Lyman- α (see text). The S/N ratio is plotted as a function of the small-scale cutoff (k_{\max}) to which the data-analysis of the survey extends. Given that the ratio grows with the number of small scale modes and then reaches a saturation point suggests that the S/N of the relativistic effects is dominated by the shot-noise, and not by the cosmic variance. However, no systematic effects have been included in our analysis, and it is likely that in the real data, the signal is dominated by the systematics (see text for details).

We plot the signal-to-noise as a function of the small-scale cutoff k_{\max} in Fig. 9. We are showing the results for current BOSS survey (in red) and future DESI survey (in blue).

The shaded regions represent the uncertainty in the S/N ratio, when allowing for the values of evolution and magnification biases to vary ($f_{\text{evo}}^{\text{Ly}\alpha}$, f_{evo}^Q and s). The values

were taken to be the same as in Fig. 7 and 8. The boundary lines of the shaded region correspond to +5% ($f_{\text{evo}}^{\text{Ly}\alpha} = -3.15$, $f_{\text{evo}}^{\text{Q}} = 6.19163$, $s = 0.256883$ - top line) and -5% ($f_{\text{evo}}^{\text{Ly}\alpha} = -2.85$, $f_{\text{evo}}^{\text{Q}} = 4.74261$, $s = 0.450115$ - bottom line) changes in evolution biases. The above values were taken to be the same for both BOSS and DESI surveys. While the uncertainty of the values for evolution biases (or other bias factors) remains a source of a systematic error for the future measurements, it does not significantly change the ability to measure the relativistic effects.

The values for the noise power estimates used for the BOSS survey were obtained using the relations presented in [10, 45], where the Lyman- α noise power is given by the one-dimensional power spectrum multiplied by the effective density of lines of sight per unit area n_{eff} :

$$N_{\alpha}^{\text{BOSS}} = P_{\alpha}^{1D}(k\mu)n_{\text{eff}}^{-1}. \quad (4.36)$$

The one-dimensional Lyman- α power spectrum was obtained by integration of P_{α} given by Eq. (4.31). The value of density of lines of sight was estimated for BOSS to be $n_{\text{eff}} = 10^{-3} (h^{-1}\text{Mpc})^{-2}$. Evaluating at a typical scale and angle ($k = 0.14 h \text{ Mpc}^{-1}$, $\mu = k_{\parallel}/k = 0.6$) we acquire the value of $N_{\alpha}^{\text{BOSS}} = 2670 (h^{-1}\text{Mpc})^3$. For the QSO noise we assume that it is given by the number density of the QSOs in the survey. For BOSS we use the values of 164,017 number of quasars over 8,976 square degrees, in the redshift range of $z = 2 - 3.5$.

For DESI we use the data presented in [46]. The noise for the Lyman- α forest is estimated to be $nP_{\alpha}(k = 0.14 h \text{ Mpc}^{-1}, \mu = 0.6) = 0.09$, which gives $N_{\alpha}^{\text{DESI}} = 272 (h^{-1}\text{Mpc})^3$. The quasar noise was estimated using the table of QSO redshift distribution, in the redshift range $z = 1.96 - 3.55$, resulting in 787,227 quasars over 14,000 square degrees.

The results shown in Fig. 9 show that in both surveys the signal of the relativistic effects is shot-noise dominated, with both achieving their maximum values at around $k_{\text{max}} = 0.1 h \text{ Mpc}^{-1}$. The value for BOSS survey is low, $S/N \sim 1.4$, indicating that the relativistic effects cannot be measured with high significance, but they would still be an important systematic effect. It is also likely that they might be identified as continuum systematic effects, with which they are likely degenerate to some extent (see the following section for details).

For DESI however, the results are much more promising, giving $S/N \sim 7.2$, suggesting that future surveys would be able to see this effect. However, we caution the reader that this analysis was very simple, especially in the sense that it did not involve any systematic effects. Measurements of the BOSS QSO-Lyman- α cross-correlations ([9, 10]) have shown that the uncertainties are dominated by the systematic effects, which need to be carefully modeled. We claim however, that relativistic effects need to be included in such analysis as they are an important correction to the over signal.

4.5 Discussion on systematic effects

Two of the major concerns about measuring the relativistic effects are the possible degeneracy with other physical processes (e.g. primordial non-gaussianity, UV background

fluctuations), and the effect of systematic uncertainties in the data induced by the data-analysis process (e.g. continuum fitting, redshift errors). In this section we characterize the main sources of these uncertainties and discuss on their possible impact on the results of our paper.

The largest source of systematic uncertainties comes from the inability to clearly separate the QSO intrinsic continuum level and mean absorption (and its fluctuations) in the Lyman- α forest region. The exact systematic effects from the continuum fitting depend on the data-analysis technique as well as the continuum estimation method, and would require a very careful survey-specific analysis to carefully check what are the targeted uncertainties allowed in the continuum fitting to be able to measure the relativistic effects presented in this paper. This is well beyond the scope of this paper.

However, in the following we present a rough estimation of the required continuum estimations. The continuum fitting procedure affects the measured QSO-Lyman- α cross-correlation because of the inability to clearly separate the continuum and Lyman- α forest large scale fluctuations. This manifests itself as a scale dependent continuum fluctuation dominated by large scales. These distortion effects have been considered before (see [10]) and may potentially mimic the relativistic signal. The theoretical models used to account for such distortions ([8, 10]) predict an asymmetric distortion to the cross-correlation function with slight dependence on the coordinate along the line of sight. However the values are much below the relativistic signals.

On the other hand successive measurements of the BOSS QSO-Lyman- α cross-correlation ([9, 10]) have shown that the final uncertainties are strongly dominated by the continuum systematic effects. In a very simple picture where the continuum uncertainties come from a mere wrong normalization of the continuum (i.e. zero-mode of the continuum fluctuations) it would produce a multiplicative offset in the cross-correlation function. As the relativistic corrections seem to apply a nearly constant distortion above $\sim 40 h^{-1}\text{Mpc}$, they can be mimicked by a wrong continuum level. Whereas the relativistic effects are asymmetric, a mere wrong continuum level would introduce a symmetric offset. As a rough estimation the continuum level in the future surveys must be known to a better than a few percent level, if a high-significance measurement of the relativistic effects is to be achieved.

As shown in [9], the quasar redshift errors would shift the whole correlation function for a constant amount, while also smearing the small scales due to the variance of the redshift estimates. A systematic shift of the redshift of the quasars would imply an incorrect wavelength calibration of the quasar spectra. This would in turn mean that the redshifts of the Lyman- α forest are also systematically offset for the same amount (Δ_z). Combining the above generates a coordinate translation of the kind $\langle \Delta_Q(z_1)\delta_F(z_2) \rangle \rightarrow \langle \Delta_Q(z_1 - \Delta_z)\delta_F(z_2 - \Delta_z) \rangle$. This is exactly how the effect was modelled in [9], where the theoretical correlation function was convolved with a gaussian profile, with the mean corresponding to Δ_z and a width corresponding to the variance of redshift estimates. Such a translation would only shift the whole cross-correlation function, so that its peak would be at Δ_z and not at $z_2 - z_1 = 0$. The shape would not be changed (except on small scales due to the smearing of the kernel function), and would not change

the signal of the asymmetric cross-correlation function.

Another important systematic effect inherent to data-analysis of the Lyman- α forest is the inability to properly filter out metal contaminants that are falsely identified as Lyman- α absorbers. While most of these metal contaminants only affect small scales of the Lyman- α forest fluctuations, there is one metal line very close to the Lyman- α line, that is known to be associated with Si III absorption. First observed and modeled in [30], it was shown that it causes a smaller, secondary maximum in the Lyman- α auto-correlation function. However, in the QSO-Lyman- α cross-correlation function such an effect would undoubtedly induce asymmetry in the cross-correlation function. To assess this systematic signal we adopt a simple model used in [30], where the contribution of the Si III to the total flux fluctuations can be modeled as shifted and rescaled Lyman- α fluctuations, $\delta_F(z) = \delta_\alpha(z) + a\delta_\alpha(z + z_3)$, where the shift due to Si II is $z_3 = v_3 \sim 0.0078$, and the scale was estimated to be $a \sim 0.044$ at $z = 2.5$. To the first order in z_3 , the correction to the overall cross-correlation function is equal to $\langle \Delta_Q \delta_F \rangle = \langle \Delta_Q \delta_\alpha \rangle + a \langle \Delta_Q \delta_\alpha \rangle + az_3 \langle \Delta_Q \partial_z \delta_\alpha \rangle$. We see that the leading (zero-th order) correction will scale with a , and thus be suppressed by more than an order of magnitude compared to the Lyman- α signal and is thus a negligible effect to our results.

One of the physical processes that might modify the behaviour of large scale fluctuations is the elusive primordial non-gaussianity, that has been extensively searched for in both galaxy surveys and cosmic microwave data [47, 48]. The models in the literature so far have focused mainly on leading order effect on the density fluctuations, where they have shown that $f_{NL} \neq 0$ generates a scale dependent density bias factor, that has a correction of the order of $(\mathcal{H}/k)^2$ to the observed over-density. This is of the same order of magnitude as our potential terms, and moreover, it is symmetric, and will thus not affect the asymmetric correlation function. Similar behaviour can be observed for the effect of UV background fluctuations. The current models ([49, 50]) show that such fluctuations change only the symmetric part (adding power only to the real part of the power spectrum). However, some second order corrections are expected from cross-correlating these symmetric effects with the leading asymmetric terms, and a more detailed analysis would be required to study the combined effects.

5 Conclusions

In this paper we have computed the relativistic effects in the Lyman- α forest in the linear regime on large scales. There are two main reasons to conduct such a study: firstly, the future surveys are going to measure the regime of large scales where the relativistic effects may become important ($\sim 10\%$ of the signal at the BAO scale), and secondly, the already existing data can be used with multiple tracers to boost specific signals beyond the standard Newtonian terms and constrain cosmological information.

Using two differently biased tracers to boost the small signal of the relativistic effects have been suggested in the past [13, 14, 18, 20, 21] but mostly in the context of different galaxy populations. Here we have adopted the approach, used the newly computed relativistic expansion for the Lyman- α forest and shown that when combining

two tracers with very different bias factors (such as Quasars and Lyman- α forest) one can enhance the desired signal.

The main effect on the cross-correlation function can be measured through an anti-symmetric part of the correlation function. We show that the relativistic effects, and most prominently the Doppler term, give rise to the most dominant contribution. While these new terms include a variety of exciting information, there are two sub-dominant effects that need to be carefully modeled: the redshift evolution of the density (and velocity-gradient) bias factors of the tracers, and the QSO lensing term. In the light of the lensing effects, the cosmological signal is strongly contaminated by the magnification, and to lesser extent, evolution bias of the QSOs. While all the bias parameters can be determined from the independent surveys it is important to note that they can mimic the effects of different cosmology or theory of gravity.

For the given configuration of the tracers the results show that the contaminating effects are surprisingly small at BAO scale. While this only reflects the specific values of the bias parameters and their redshift evolution for these two tracers, it can be used to determine the effect of the Doppler terms at the BAO scale.

Another possible advantage for the precision measurements of future surveys is to isolate the anti-symmetric signal of lensing or potential terms and use them to test the validity of the Einstein's General Relativity or constrain the modifications of the theory of gravity. The dominant signal, coming from the Doppler term, would not change under a different theory of gravity, unless the theory violates the energy-momentum tensor conservation. Even though, the potential and lensing signals are small, if measured they would provide a unique test of General Relativity on the BAO scales, thus in the regime where perturbations can be measured much better than at horizon scales.

Acknowledgement

We thank Anže Slosar and Ruth Durrer for fruitful discussions. We also thank anonymous referee for insightful suggestions. ED and MV are supported by the ERC grant 'cosmoIGM' and by INFN/PD51 INDARK grant.

A Angular power spectrum

After having computed the 2-point correlation function we can compute the power spectrum as well. Since the observables defined in Eqs. (3.25,3.17) depend on angular positions and redshifts, spherical harmonics are the natural basis to expand them as follows

$$\Delta_A(z, \mathbf{n}) = \sum_{\ell m} a_{\ell m}^A(z) Y_{\ell m}(\mathbf{n}) , \quad (\text{A.1})$$

$$a_{\ell m}^A(z) = \int d\Omega_{\mathbf{n}} \Delta_A(z, \mathbf{n}) Y_{\ell m}^*(\mathbf{n}) . \quad (\text{A.2})$$

Then, we define the redshift dependent angular power spectra

$$C_{\ell}^{AB}(z, z') = \langle a_{\ell m}^A(z) a_{\ell m}^{B*}(z') \rangle \quad (\text{A.3})$$

where A and B denotes two observables. It is convenient to write the angular power spectra in terms of integral over the angular transfer function $\Delta_\ell^A(\eta, k)$ through

$$C_\ell^{AB}(z, z') = 4\pi \int \frac{dk}{k} \Delta_\ell^A(k, \eta) \Delta_\ell^{B*}(k, \eta') \mathcal{P}_R(k), \quad (\text{A.4})$$

where $\mathcal{P}_R(k) = k^3 P_R(k) / (2\pi^2)$ is the dimensionless primordial curvature power spectrum. The same formalism has been successfully applied to Cosmic Microwave Background (CMB), Weak Lensing (WL) and galaxy clustering. Because of that, the implementation in a Boltzmann code is straightforward. In this work we have modified the public CLASS code [35, 36], in particular the part included in CLASSgal [38] and we have adopted it to computed, through Eq. (4.3), the correlation function of non-local terms.

As shown in galaxy clustering, the analysis based on redshift dependent 2-dimensional power spectra recovers the same amount of information of the traditional 3-dimensional analysis, see e.g. [17, 51, 52]. In addition, it is the natural way to include relativistic or light-cone effects and it has been already considered in several works. Hence, the formalism here discussed can be used directly to perform a 3-dimensional analysis, including all the relativistic effects to first order in perturbation theory.

Ly- α power transfer function

For the transmitted flux, from Eqs. (3.3, 3.11), we compute the angular transfer function

$$\begin{aligned} \Delta_\ell(k, \eta) = & b T_D j_\ell(kr) + b_v \mathcal{H}^{-1} T_\Theta j_\ell''(kr) \\ & + b_R \left\{ \left[\left(3 + \frac{\dot{\mathcal{H}}}{\mathcal{H}^2} - f_{\text{evo}}^{\text{Ly}\alpha} \right) T_\Psi + \mathcal{H}^{-1} T_{\dot{\Phi}} + (f_{\text{evo}}^{\text{Ly}\alpha} - 3) \frac{\mathcal{H}}{k^2} T_\Theta \right] j_\ell(kr) \right. \\ & \left. + \left(3 + \frac{\dot{\mathcal{H}}}{\mathcal{H}^2} - f_{\text{evo}}^{\text{Ly}\alpha} \right) k^{-1} T_\Theta j_\ell'(kr) + \left(2 + \frac{\dot{\mathcal{H}}}{\mathcal{H}^2} - f_{\text{evo}}^{\text{Ly}\alpha} \right) \int_0^r T_{\dot{\Psi}+\dot{\Phi}} j_\ell(kr') dr' \right\}, \end{aligned} \quad (\text{A.5})$$

where a prime denotes the derivative of the spherical Bessel functions with respect to their argument. All the quantities are evaluated at (k, η) if not written explicitly.

Quasars transfer function

Following the notation of [38], we reproduce here the angular transfer function for QSO

$$\begin{aligned}
\Delta_\ell(z, k) = & j_\ell(kr) \left[bT_D + \left(\frac{\dot{\mathcal{H}}}{\mathcal{H}^2} + \frac{2-5s}{r\mathcal{H}} + 5s - f_{\text{evo}}^Q + 1 \right) T_\Psi \right. \\
& \left. + (-2 + 5s) T_\Phi + \mathcal{H}^{-1} T_{\dot{\Phi}} \right] \\
& + \left[\frac{dj_\ell}{dx}(kr) \left(\frac{\dot{\mathcal{H}}}{\mathcal{H}^2} + \frac{2-5s}{r\mathcal{H}} + 5s - f_{\text{evo}}^Q \right) + \frac{d^2 j_\ell}{dx^2}(kr) \frac{k}{\mathcal{H}} (f_{\text{evo}}^Q - 3) j_\ell(kr) \frac{\mathcal{H}}{k} \right] T_V \\
& + \int_0^{r(z)} dr j_\ell(kr) \left[T_{\Phi+\Psi} \left(\frac{2-5s}{2} \right) \left(\ell(\ell+1) \frac{r(z)-r}{r(z)r} + \frac{2}{r(z)} \right) \right. \\
& \left. + T_{\dot{\Phi}+\dot{\Psi}} \left(\frac{\dot{\mathcal{H}}}{\mathcal{H}^2} + \frac{2-5s}{r(z)\mathcal{H}} + 5s - f_{\text{evo}}^Q \right) \right]_{r(z)}. \tag{A.6}
\end{aligned}$$

B CLASS modifications

Here we present the modified transfer function in CLASS code [35, 36], in particular for the galaxy number counts calculation developed in CLASSgal [38], where the angular power spectrum between the i -th and the j -th redshift bins is denoted by

$$c_\ell^{ij} = 4\pi \int \frac{dk}{k} \mathcal{P}_{\mathcal{R}}(k) \Delta_\ell^i(k) \Delta_\ell^j(k) \tag{B.1}$$

with

$$\begin{aligned}
\Delta_\ell(k) = & \Delta_\ell^{\text{Den}_i} && \text{(Density)} \\
& + \Delta_\ell^{\text{Red}_i} && \text{(Redshift space distortion)} \\
& + \Delta_\ell^{\text{D1}_i} + \Delta_\ell^{\text{D2}_i} && \text{(Doppler)} \\
& + \Delta_\ell^{\text{G1}_i} + \Delta_\ell^{\text{G2}_i} + \Delta_\ell^{\text{G3}_i} + \Delta_\ell^{\text{G5}_i} && \text{(Gravitational potential)} \tag{B.2}
\end{aligned}$$

and

$$\begin{aligned}
\Delta_\ell^{\text{Den}i} &= \int_0^{\eta_0} d\eta W_i b_{\text{SD}} j_\ell \\
\Delta_\ell^{\text{Red}i} &= \int_0^{\eta_0} d\eta W_i \frac{b_v}{aH} S_\Theta \frac{d^2 j_\ell}{dx^2} \\
\Delta_\ell^{\text{D1}i} &= \int_0^{\eta_0} d\eta W_i \frac{4 + \frac{\dot{H}}{aH^2} - f_{\text{evo}}^{\text{Ly}\alpha}}{k} S_\Theta b_R \frac{dj_\ell}{dx} \\
\Delta_\ell^{\text{D2}i} &= \int_0^{\eta_0} d\eta W_i (f_{\text{evo}}^{\text{Ly}\alpha} - 3) \frac{aH}{k^2} S_\Theta b_R j_\ell \\
\Delta_\ell^{\text{G1}i} &= \int_0^{\eta_0} d\eta W_i S_\Psi b_R j_\ell \\
\Delta_\ell^{\text{G2}i} &= - \int_0^{\eta_0} d\eta W_i \left(3 + \frac{\dot{H}}{aH^2} - f_{\text{evo}}^{\text{Ly}\alpha} \right) S_\Phi b_R j_\ell \\
\Delta_\ell^{\text{G3}i} &= \int_0^{\eta_0} d\eta W_i \frac{1}{aH} S_\Phi b_R j_\ell \\
\Delta_\ell^{\text{G5}i} &= \int_0^{\eta_0} d\eta W_i^{\text{G5}} S_{(\Phi+\Psi)} k \frac{dj_\ell}{dx}, \tag{B.3}
\end{aligned}$$

where W_i denotes the selection function of the i -th redshift bin of the survey. We have omitted all the arguments: k for the transfer functions, (η, k) for the source functions, $x \equiv k(\eta_0 - \eta)$ for the Bessel functions, and η for selection and background functions. For the integrated term G5, we have defined

$$W_i^{\text{G5}}(\eta) = \int_0^\eta d\tilde{\eta} b_R W_i(\tilde{\eta}) \left(3 + \frac{\dot{H}}{aH^2} - f_{\text{evo}}^{\text{Ly}\alpha} \right)_{\tilde{\eta}}.$$

The term G4 vanishes because of the absence of time-delay effect in Lyman- α observable.

References

- [1] M. Rauch, *The Lyman Alpha Forest in the Spectra of QSOs*, ARAA **36** (1998) 267–316, [[astro-ph/9806286](#)].
- [2] A. A. Meiksin, *The physics of the intergalactic medium*, Reviews of Modern Physics **81** (Oct., 2009) 1405–1469, [[arXiv:0711.3358](#)].
- [3] N. G. Busca, T. Delubac, J. Rich, S. Bailey, A. Font-Ribera, D. Kirkby, J.-M. Le Goff, M. M. Pieri, A. Slosar, É. Aubourg, J. E. Bautista, D. Bizyaev, M. Blomqvist, A. S. Bolton, J. Bovy, H. Brewington, A. Borde, J. Brinkmann, B. Carithers, R. A. C. Croft, K. S. Dawson, G. Ebelke, D. J. Eisenstein, J.-C. Hamilton, S. Ho, D. W. Hogg, K. Honscheid, K.-G. Lee, B. Lundgren, E. Malanushenko, V. Malanushenko, D. Margala, C. Maraston, K. Mehta, J. Miralda-Escudé, A. D. Myers, R. C. Nichol, P. Noterdaeme, M. D. Olmstead, D. Oravetz, N. Palanque-Delabrouille, K. Pan, I. Pâris, W. J. Percival, P. Petitjean, N. A. Roe, E. Rollinde, N. P. Ross, G. Rossi, D. J. Schlegel, D. P. Schneider,

- A. Sheldon, E. S. Sheldon, A. Simmons, S. Snedden, J. L. Tinker, M. Viel, B. A. Weaver, D. H. Weinberg, M. White, C. Yèche, and D. G. York, *Baryon acoustic oscillations in the Ly α forest of BOSS quasars*, *A&A* **552** (Apr., 2013) A96, [[arXiv:1211.2616](#)].
- [4] A. Slosar, V. Iršič, D. Kirkby, S. Bailey, N. G. Busca, T. Delubac, J. Rich, É. Aubourg, J. E. Bautista, V. Bhardwaj, M. Blomqvist, A. S. Bolton, J. Bovy, J. Brownstein, B. Carithers, R. A. C. Croft, K. S. Dawson, A. Font-Ribera, J.-M. Le Goff, S. Ho, K. Honscheid, K.-G. Lee, D. Margala, P. McDonald, B. Medolin, J. Miralda-Escudé, A. D. Myers, R. C. Nichol, P. Noterdaeme, N. Palanque-Delabrouille, I. Pâris, P. Petitjean, M. M. Pieri, Y. Piškur, N. A. Roe, N. P. Ross, G. Rossi, D. J. Schlegel, D. P. Schneider, N. Suzuki, E. S. Sheldon, U. Seljak, M. Viel, D. H. Weinberg, and C. Yèche, *Measurement of baryon acoustic oscillations in the Lyman- α forest fluctuations in BOSS data release 9*, *JCAP* **4** (Apr., 2013) 26, [[arXiv:1301.3459](#)].
- [5] N. Palanque-Delabrouille, C. Yèche, A. Borde, J.-M. Le Goff, G. Rossi, M. Viel, É. Aubourg, S. Bailey, J. Bautista, M. Blomqvist, A. Bolton, J. S. Bolton, N. G. Busca, B. Carithers, R. A. C. Croft, K. S. Dawson, T. Delubac, A. Font-Ribera, S. Ho, D. Kirkby, K.-G. Lee, D. Margala, J. Miralda-Escudé, D. Muna, A. D. Myers, P. Noterdaeme, I. Pâris, P. Petitjean, M. M. Pieri, J. Rich, E. Rollinde, N. P. Ross, D. J. Schlegel, D. P. Schneider, A. Slosar, and D. H. Weinberg, *The one-dimensional Ly α forest power spectrum from BOSS*, *A&A* **559** (Nov., 2013) A85, [[arXiv:1306.5896](#)].
- [6] N. Palanque-Delabrouille, C. Yèche, J. Baur, C. Magneville, G. Rossi, J. Lesgourgues, A. Borde, E. Burtin, J.-M. LeGoff, J. Rich, M. Viel, and D. Weinberg, *Cosmology with Lyman-alpha forest power spectrum*, *ArXiv e-prints* (June, 2015) [[arXiv:1506.05976](#)].
- [7] M. Viel, G. D. Becker, J. S. Bolton, and M. G. Haehnelt, *Warm dark matter as a solution to the small scale crisis: New constraints from high redshift Lyman- α forest data*, *Phys. Rev. D* **88** (Aug., 2013) 043502, [[arXiv:1306.2314](#)].
- [8] A. Font-Ribera, J. Miralda-Escudé, E. Arnau, B. Carithers, K.-G. Lee, P. Noterdaeme, I. Pâris, P. Petitjean, J. Rich, E. Rollinde, N. P. Ross, D. P. Schneider, M. White, and D. G. York, *The large-scale cross-correlation of Damped Lyman alpha systems with the Lyman alpha forest: first measurements from BOSS*, *JCAP* **11** (Nov., 2012) 59, [[arXiv:1209.4596](#)].
- [9] A. Font-Ribera, E. Arnau, J. Miralda-Escudé, E. Rollinde, J. Brinkmann, J. R. Brownstein, K.-G. Lee, A. D. Myers, N. Palanque-Delabrouille, I. Pâris, P. Petitjean, J. Rich, N. P. Ross, D. P. Schneider, and M. White, *The large-scale quasar-Lyman α forest cross-correlation from BOSS*, *JCAP* **5** (May, 2013) 18, [[arXiv:1303.1937](#)].
- [10] A. Font-Ribera, D. Kirkby, N. Busca, J. Miralda-Escudé, N. P. Ross, A. Slosar, J. Rich, É. Aubourg, S. Bailey, V. Bhardwaj, J. Bautista, F. Beutler, D. Bizyaev, M. Blomqvist, H. Brewington, J. Brinkmann, J. R. Brownstein, B. Carithers, K. S. Dawson, T. Delubac, G. Ebelke, D. J. Eisenstein, J. Ge, K. Kinemuchi, K.-G. Lee, V. Malanushenko, E. Malanushenko, M. Marchante, D. Margala, D. Muna, A. D. Myers, P. Noterdaeme, D. Oravetz, N. Palanque-Delabrouille, I. Pâris, P. Petitjean, M. M. Pieri, G. Rossi, D. P. Schneider, A. Simmons, M. Viel, C. Yèche, and D. G. York, *Quasar-Lyman α forest cross-correlation from BOSS DR11: Baryon Acoustic Oscillations*, *JCAP* **5** (May, 2014) 27, [[arXiv:1311.1767](#)].
- [11] K. S. Dawson, J.-P. Kneib, W. J. Percival, S. Alam, F. D. Albareti, S. F. Anderson, E. Armengaud, E. Aubourg, S. Bailey, J. E. Bautista, A. A. Berlind, M. A. Bershadsky, F. Beutler, D. Bizyaev, M. R. Blanton, M. Blomqvist, A. S. Bolton, J. Bovy, W. N.

- Brandt, J. Brinkmann, J. R. Brownstein, E. Burtin, N. G. Busca, Z. Cai, C.-H. Chuang, N. Clerc, J. Comparat, F. Cope, R. A. C. Croft, I. Cruz-Gonzalez, L. N. da Costa, M.-C. Cousinou, J. Darling, S. de la Torre, T. Delubac, H. du Mas des Bourboux, T. Dwelly, A. Ealet, D. J. Eisenstein, M. Eracleous, S. Escoffier, X. Fan, A. Finoguenov, A. Font-Ribera, P. Frinchaboy, P. Gaulme, A. Georgakakis, P. Green, H. Guo, J. Guy, S. Ho, D. Holder, J. Huehnerhoff, T. Hutchinson, Y. Jing, E. Jullo, V. Kamble, K. Kinemuchi, D. Kirkby, F.-S. Kitaura, M. A. Klaene, R. R. Laher, D. Lang, P. Laurent, J.-M. Le Goff, C. Li, Y. Liang, M. Lima, Q. Lin, W. Lin, Y.-T. Lin, D. C. Long, B. Lundgren, N. MacDonald, M. A. Geimba Maia, E. Malanushenko, V. Malanushenko, V. Mariappan, C. K. McBride, I. D. McGreer, B. Menard, A. Merloni, A. Meza, A. D. Montero-Dorta, D. Muna, A. D. Myers, K. Nandra, T. Naugle, J. A. Newman, P. Noterdaeme, P. Nugent, R. Ogando, M. D. Olmstead, A. Oravetz, D. J. Oravetz, N. Padmanabhan, N. Palanque-Delabrouille, K. Pan, J. K. Parejko, I. Paris, J. A. Peacock, P. Petitjean, M. M. Pieri, A. Pisani, F. Prada, A. Prakash, A. Raichoor, B. Reid, J. Rich, J. Ridl, S. Rodriguez-Torres, A. Carnero Rosell, A. J. Ross, G. Rossi, J. Ruan, M. Salvato, C. Sayres, D. P. Schneider, D. J. Schlegel, U. Seljak, H.-J. Seo, B. Sesar, S. Shandera, Y. Shu, A. Slosar, F. Sobreira, M. A. Strauss, A. Streblyanska, N. Suzuki, C. Tao, J. L. Tinker, R. Tojeiro, M. Vargas-Magana, Y. Wang, B. A. Weaver, D. H. Weinberg, M. White, W. M. Wood-Vasey, C. Yeche, Z. Zhai, C. Zhao, G.-b. Zhao, Z. Zheng, G. Ben Zhu, and H. Zou, *The SDSS-IV extended Baryon Oscillation Spectroscopic Survey: Overview and Early Data*, ArXiv e-prints (Aug., 2015) [[arXiv:1508.04473](#)].
- [12] M. Levi, C. Bebek, T. Beers, R. Blum, R. Cahn, D. Eisenstein, B. Flaugher, K. Honscheid, R. Kron, O. Lahav, P. McDonald, N. Roe, D. Schlegel, and representing the DESI collaboration, *The DESI Experiment, a whitepaper for Snowmass 2013*, ArXiv e-prints (Aug., 2013) [[arXiv:1308.0847](#)].
- [13] P. McDonald, *Gravitational redshift and other redshift-space distortions of the imaginary part of the power spectrum*, JCAP **0911** (2009) 026, [[arXiv:0907.5220](#)].
- [14] J. Yoo, N. Hamaus, U. Seljak, and M. Zaldarriaga, *Going beyond the Kaiser redshift-space distortion formula: a full general relativistic account of the effects and their detectability in galaxy clustering*, Phys. Rev. **D86** (2012) 063514, [[arXiv:1206.5809](#)].
- [15] J. Yoo and U. Seljak, *Wide Angle Effects in Future Galaxy Surveys*, Mon. Not. Roy. Astron. Soc. **447** (2015), no. 2 1789–1805, [[arXiv:1308.1093](#)].
- [16] R. A. C. Croft, *Gravitational redshifts from large-scale structure*, MNRAS **434** (Oct., 2013) 3008–3017, [[arXiv:1304.4124](#)].
- [17] E. Di Dio, F. Montanari, R. Durrer, and J. Lesgourgues, *Cosmological Parameter Estimation with Large Scale Structure Observations*, JCAP **1401** (2014) 042, [[arXiv:1308.6186](#)].
- [18] C. Bonvin, L. Hui, and E. Gaztanaga, *Asymmetric galaxy correlation functions*, Phys. Rev. **D89** (2014), no. 8 083535, [[arXiv:1309.1321](#)].
- [19] D. Alonso, P. Bull, P. G. Ferreira, R. Maartens, and M. G. Santos, *Ultra-large-scale Cosmology in Next-generation Experiments with Single Tracers*, ApJ **814** (Dec., 2015) 145, [[arXiv:1505.07596](#)].
- [20] D. Alonso and P. G. Ferreira, *Constraining ultralarge-scale cosmology with multiple tracers in optical and radio surveys*, Phys. Rev. D **92** (Sept., 2015) 063525, [[arXiv:1507.03550](#)].

- [21] J. Fonseca, S. Camera, M. G. Santos, and R. Maartens, *Hunting Down Horizon-scale Effects with Multi-wavelength Surveys*, ApJL **812** (Oct., 2015) L22, [[arXiv:1507.04605](#)].
- [22] A. Arinyo-i-Prats, J. Miralda-Escudé, M. Viel, and R. Cen, *The Non-Linear Power Spectrum of the Lyman Alpha Forest*, ArXiv e-prints (June, 2015) [[arXiv:1506.04519](#)].
- [23] A. Slosar, A. Font-Ribera, M. M. Pieri, J. Rich, J.-M. Le Goff, É. Aubourg, J. Brinkmann, N. Busca, B. Carithers, R. Charlassier, M. Cortès, R. Croft, K. S. Dawson, D. Eisenstein, J.-C. Hamilton, S. Ho, K.-G. Lee, R. Lupton, P. McDonald, B. Medolin, D. Muna, J. Miralda-Escudé, A. D. Myers, R. C. Nichol, N. Palanque-Delabrouille, I. Pâris, P. Petitjean, Y. Piškur, E. Rollinde, N. P. Ross, D. J. Schlegel, D. P. Schneider, E. Sheldon, B. A. Weaver, D. H. Weinberg, C. Yeche, and D. G. York, *The Lyman- α forest in three dimensions: measurements of large scale flux correlations from BOSS 1st-year data*, JCAP **9** (Sept., 2011) 1, [[arXiv:1104.5244](#)].
- [24] P. McDonald, *Toward a Measurement of the Cosmological Geometry at $z \sim 2$: Predicting Ly α Forest Correlation in Three Dimensions and the Potential of Future Data Sets*, ApJ **585** (Mar., 2003) 34–51, [[astro-ph/0108064](#)].
- [25] C. Bonvin and R. Durrer, *What galaxy surveys really measure*, Phys. Rev. **D84** (2011) 063505, [[arXiv:1105.5280](#)].
- [26] **Planck** Collaboration, P. A. R. Ade et al., *Planck 2015 results. XIII. Cosmological parameters*, [arXiv:1502.01589](#).
- [27] A. Challinor and A. Lewis, *The linear power spectrum of observed source number counts*, Phys. Rev. **D84** (2011) 043516, [[arXiv:1105.5292](#)].
- [28] U. Seljak, *Bias, redshift space distortions and primordial nongaussianity of nonlinear transformations: application to Ly- α forest*, JCAP **3** (Mar., 2012) 4, [[arXiv:1201.0594](#)].
- [29] A. M. Cieplak and A. Slosar, *Towards physics responsible for large-scale Lyman- α forest bias parameters*, ArXiv e-prints (Sept., 2015) [[arXiv:1509.07875](#)].
- [30] P. McDonald, U. Seljak, S. Burles, D. J. Schlegel, D. H. Weinberg, R. Cen, D. Shih, J. Schaye, D. P. Schneider, N. A. Bahcall, J. W. Briggs, J. Brinkmann, R. J. Brunner, M. Fukugita, J. E. Gunn, Ž. Ivezić, S. Kent, R. H. Lupton, and D. E. Vanden Berk, *The Ly α Forest Power Spectrum from the Sloan Digital Sky Survey*, ApJS **163** (Mar., 2006) 80–109, [[astro-ph/0405013](#)].
- [31] S. M. Croom, B. J. Boyle, T. Shanks, R. J. Smith, L. Miller, P. J. Outram, N. S. Loaring, F. Hoyle, and J. da Ângela, *The 2dF QSO Redshift Survey - XIV. Structure and evolution from the two-point correlation function*, MNRAS **356** (Jan., 2005) 415–438, [[astro-ph/0409314](#)].
- [32] A. D. Myers, R. J. Brunner, R. C. Nichol, G. T. Richards, D. P. Schneider, and N. A. Bahcall, *Clustering Analyses of 300,000 Photometrically Classified Quasars. I. Luminosity and Redshift Evolution in Quasar Bias*, ApJ **658** (Mar., 2007) 85–98, [[astro-ph/0612190](#)].
- [33] M. White, A. D. Myers, N. P. Ross, D. J. Schlegel, J. F. Hennawi, Y. Shen, I. McGreer, M. A. Strauss, A. S. Bolton, J. Bovy, X. Fan, J. Miralda-Escudé, N. Palanque-Delabrouille, I. Paris, P. Petitjean, D. P. Schneider, M. Viel, D. H. Weinberg, C. Yeche, I. Zehavi, K. Pan, S. Snedden, D. Bizyaev, H. Brewington, J. Brinkmann, V. Malanushenko, E. Malanushenko, D. Oravetz, A. Simmons, A. Sheldon, and B. A. Weaver, *The clustering of intermediate-redshift quasars as measured by the Baryon Oscillation Spectroscopic Survey*, MNRAS **424** (Aug., 2012) 933–950, [[arXiv:1203.5306](#)].

- [34] N. P. Ross, I. D. McGreer, M. White, G. T. Richards, A. D. Myers, N. Palanque-Delabrouille, M. A. Strauss, S. F. Anderson, Y. Shen, W. N. Brandt, C. Yèche, M. E. C. Swanson, É. Aubourg, S. Bailey, D. Bizyaev, J. Bovy, H. Brewington, J. Brinkmann, C. DeGraf, T. Di Matteo, G. Ebelke, X. Fan, J. Ge, E. Malanushenko, V. Malanushenko, R. Mandelbaum, C. Maraston, D. Muna, D. Oravetz, K. Pan, I. Pâris, P. Petitjean, K. Schawinski, D. J. Schlegel, D. P. Schneider, J. D. Silverman, A. Simmons, S. Snedden, A. Streblyanska, N. Suzuki, D. H. Weinberg, and D. York, *The SDSS-III Baryon Oscillation Spectroscopic Survey: The Quasar Luminosity Function from Data Release Nine*, ApJ **773** (Aug., 2013) 14, [[arXiv:1210.6389](#)].
- [35] J. Lesgourgues, *The Cosmic Linear Anisotropy Solving System (CLASS) I: Overview*, [arXiv:1104.2932](#).
- [36] D. Blas, J. Lesgourgues, and T. Tram, *The Cosmic Linear Anisotropy Solving System (CLASS) II: Approximation schemes*, JCAP **1107** (2011) 034, [[arXiv:1104.2933](#)].
- [37] M. LoVerde and N. Afshordi, *Extended Limber Approximation*, Phys. Rev. **D78** (2008) 123506, [[arXiv:0809.5112](#)].
- [38] E. Di Dio, F. Montanari, J. Lesgourgues, and R. Durrer, *The CLASSgal code for Relativistic Cosmological Large Scale Structure*, JCAP **1311** (2013) 044, [[arXiv:1307.1459](#)].
- [39] A. Raccanelli, D. Bertacca, R. Maartens, C. Clarkson, and O. Doré, *Lensing and time-delay contributions to galaxy correlations*, [arXiv:1311.6813](#).
- [40] F. Montanari and R. Durrer, *Measuring the lensing potential with tomographic galaxy number counts*, JCAP **10** (Oct., 2015) 070, [[arXiv:1506.01369](#)].
- [41] U. Seljak, *Extracting primordial non-gaussianity without cosmic variance*, Phys. Rev. Lett. **102** (2009) 021302, [[arXiv:0807.1770](#)].
- [42] U. Seljak, N. Hamaus, and V. Desjacques, *How to suppress the shot noise in galaxy surveys*, Phys. Rev. Lett. **103** (2009) 091303, [[arXiv:0904.2963](#)].
- [43] J. S. Bolton, M. G. Haehnelt, M. Viel, and V. Springel, *The Lyman α forest opacity and the metagalactic hydrogen ionization rate at $z \sim 2-4$* , MNRAS **357** (Mar., 2005) 1178–1188, [[astro-ph/0411072](#)].
- [44] E. Puchwein, J. S. Bolton, M. G. Haehnelt, P. Madau, G. D. Becker, and F. Haardt, *The photoheating of the intergalactic medium in synthesis models of the UV background*, MNRAS **450** (July, 2015) 4081–4097, [[arXiv:1410.1531](#)].
- [45] M. McQuinn and M. White, *On estimating Ly α forest correlations between multiple sightlines*, MNRAS **415** (Aug., 2011) 2257–2269, [[arXiv:1102.1752](#)].
- [46] A. Font-Ribera, P. McDonald, N. Mostek, B. A. Reid, H.-J. Seo, and A. Slosar, *DESI and other Dark Energy experiments in the era of neutrino mass measurements*, JCAP **5** (May, 2014) 23, [[arXiv:1308.4164](#)].
- [47] A. J. Ross, W. J. Percival, A. Carnero, G.-b. Zhao, M. Manera, A. Raccanelli, E. Aubourg, D. Bizyaev, H. Brewington, J. Brinkmann, J. R. Brownstein, A. J. Cuesta, L. A. N. da Costa, D. J. Eisenstein, G. Ebelke, H. Guo, J.-C. Hamilton, M. V. Magaña, E. Malanushenko, V. Malanushenko, C. Maraston, F. Montesano, R. C. Nichol, D. Oravetz, K. Pan, F. Prada, A. G. Sánchez, L. Samushia, D. J. Schlegel, D. P. Schneider, H.-J. Seo, A. Sheldon, A. Simmons, S. Snedden, M. E. C. Swanson, D. Thomas, J. L. Tinker, R. Tojeiro, and I. Zehavi, *The clustering of galaxies in the*

- SDSS-III DR9 Baryon Oscillation Spectroscopic Survey: constraints on primordial non-Gaussianity*, MNRAS **428** (Jan., 2013) 1116–1127, [[arXiv:1208.1491](#)].
- [48] Planck Collaboration, P. A. R. Ade, N. Aghanim, M. Arnaud, F. Arroja, M. Ashdown, J. Aumont, C. Baccigalupi, M. Ballardini, A. J. Banday, and et al., *Planck 2015 results. XVII. Constraints on primordial non-Gaussianity*, ArXiv e-prints (Feb., 2015) [[arXiv:1502.01592](#)].
- [49] S. G. A. Gontcho, J. Miralda-Escudé, and N. G. Busca, *On the effect of the ionising background on the Ly α forest autocorrelation function*, ArXiv e-prints (Apr., 2014) [[arXiv:1404.7425](#)].
- [50] A. Pontzen, S. Bird, H. Peiris, and L. Verde, *Constraints on Ionizing Photon Production from the Large-scale Ly α Forest*, ApJL **792** (Sept., 2014) L34, [[arXiv:1407.6367](#)].
- [51] J. Asorey, M. Crocce, E. Gaztanaga, and A. Lewis, *Recovering 3D clustering information with angular correlations*, Mon. Not. Roy. Astron. Soc. **427** (2012) 1891, [[arXiv:1207.6487](#)].
- [52] A. Nicola, A. Refregier, A. Amara, and A. Paranjape, *Three-dimensional spherical analyses of cosmological spectroscopic surveys*, Phys. Rev. **D90** (2014), no. 6 063515, [[arXiv:1405.3660](#)].